The International Journal of Advanced Manufacturing Technology (2022) 121:29–57
https://doi.org/10.1007/s00170-022-09365-z

CRITICAL REVIEW

Non-traditional machining techniques for silicon wafers

Noor Dzulaikha Daud[1] · Md. Nazibul Hasan[1] · Tanveer Saleh[2] · Pei Ling Leow[1] · Mohamed Sultan Mohamed Ali[1]

Received: 9 October 2021 / Accepted: 10 May 2022 / Published online: 25 May 2022
© The Author(s), under exclusive licence to Springer-Verlag London Ltd., part of Springer Nature 2022

Abstract

Silicon (Si) micromachining techniques have recently witnessed significant advancement, attributable to the high surge in demand for microelectromechanical and microelectronic devices. Micromachining techniques are widely used to cut or pattern Si, in order to obtain high-quality surface finishes for the fabrication of devices. Micromachining techniques are used for the fabrication of three-dimensional (3D) microstructures for microelectromechanical devices. In this work, the capabilities and competencies of non-traditional Si micromachining techniques, including ultrasonic, ion beam milling, laser machining, and electrical discharge machining, are discussed and compared accordingly. The working principles, advantages, limitations, and Si microstructures that have been fabricated before are discussed in detail. Additionally, this work covers the performance reported by multiple researchers on these micromachining methods, spanning the temporal range of 1990 to 2020. The key outcomes of this study are explored and summarized.

Keywords Micromachining · Silicon · Ultrasonic · Ion beam · Laser · Electrical discharge · Machining performances

1 Introduction

Micromachining has become an essential technique for the manufacturing of miniature sensors, actuators, and microsystems [1, 2]. In addition, it has also been used to fabricate three-dimensional (3D) microstructures and became a foundation of microelectromechanical systems (MEMS). MEMS uses the foundations of semiconductor integrated circuits technologies, of which, Silicon (Si) has been adopted as a structural material for MEMS devices. Although microelectronics fabrication processes, such as photolithography, thin-film deposition, chemical etching, deep reactive-ion etching, metal-assisted chemical etching, and vapor–liquid-solid are widely used for Si structure formation, the need for other 3D high aspect ratio structures have become a catalyst for the development and the use of new machining techniques. The use of machining techniques has been steadily increasingly to create the desired shapes or patterns with a certain degree of precision and surface quality, for various applications [3, 4]. Usually, the machining processes can be divided into two main categories: traditional and non-traditional machining methods, as shown in Fig. 1. Traditional machining methods can be categorized based on the cutting action (turning, milling, boring and others) and mechanical abrasion (grinding, honing, polishing and others). Nevertheless, these methods have certain limitations, such as direct contact with the machined surface, difficulties to machine hard materials, and limitations for the generation of complex geometries [3]. In contrast, non-traditional machining techniques such as ultrasonic machining (USM), ion beam milling (IBM), laser beam machining (LBM) and electrical discharge machining (EDM), have been developed to overcome these limitations by producing 3D shapes on both hard and soft materials, without direct contact with the work piece surface, resulting in less stress, high aspect ratio patterns, and relatively fast machining times [5, 6]. These techniques have been widely adopted to machine high-precision components with very restrictive dimensional and geometrical tolerances [5]. Such techniques have been well established and enabled to fabricate complex 3D Si structures, with a wide range of feature sizes, which are essential for MEMS and other microdevices.

With the objective of comprehensively illustrating the substantial progress made in the field of Si machining techniques,

✉ Mohamed Sultan Mohamed Ali
sultan_ali@fke.utm.my

[1] School of Electrical Engineering, Faculty of Engineering, Universiti Teknologi Malaysia, Johor Bahru, Johor 81310, Malaysia

[2] Department of Mechatronics Engineering, Kulliyyah of Engineering, International Islamic University Malaysia, Jalan Gombak, Kuala Lumpur 53100, Malaysia

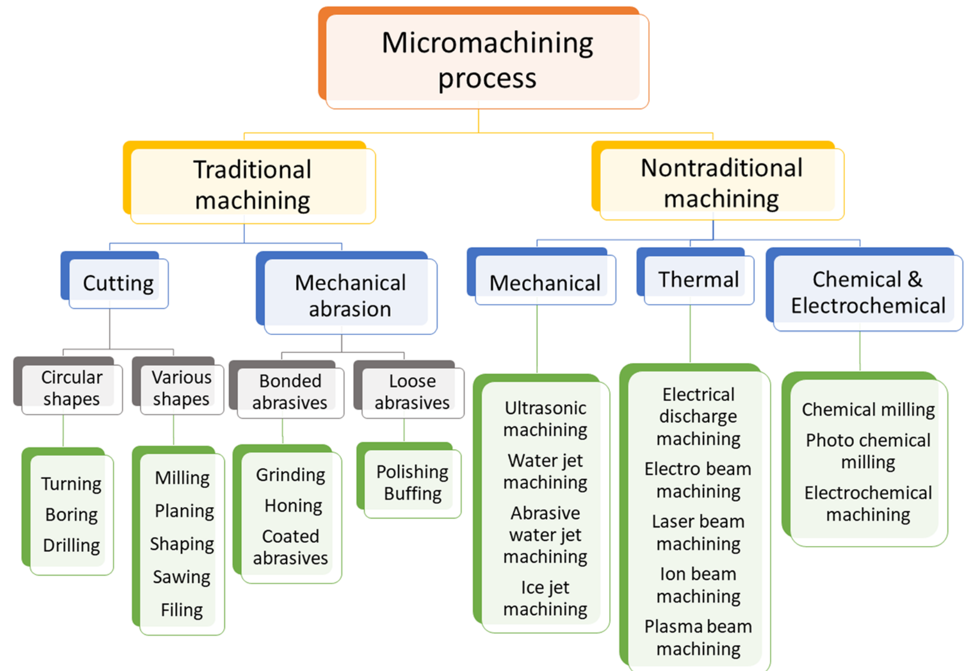

Fig. 1 Micromachining process classification. Source: own authors

non-traditional machining techniques such as USM, IBM, LBM and EDM are explored compendiously. This review covers the machining principles, beneficial features, and limitations of each technique. Additionally, this work addresses machining performance with regard to material removal rate (MRR), surface finishing quality, and the energy requirements of each of the machining techniques. Moreover, potential advantageous features and limitations of the individual techniques, as well as the performance comparisons between the non-traditional micromachining techniques, are also discussed. Eventually, the review is concluded with a discussion of the main findings of these machining techniques, towards future improvements and developments for achieving high quality and performance results.

2 Non-traditional machining techniques of Si wafers

The following section emphasizes the machining technologies for Si, focusing on selected non-traditional machining techniques, including USM, IBM, LBM and EDM. The working principles of such techniques and the performances for the machining of Si are discussed.

2.1 Ultrasonic machining

USM, also known as impact grinding or slurry drilling, relies on abrasive slurry that moves freely between the tool and workpiece. This machining technology has been used in various industries, such as aerospace, optics, and automotive [7, 8]. The first USM devices were produced in 1953–1954, and were placed on the bodies of drilling and milling machines [9]. Later, in 1960, independent USM tools were used for regular production in a variety of applications [10]. USM is a type of non-traditional machining method, that operates by vibration of a tool to produce mechanical removal processes, assisted by an abrasive slurry and liquid, in between the tool and workpiece, as can be seen in Fig. 2 [9, 11, 12]. The abrasive slurry is a mixture of irregularly-formed fine abrasive particles, such as boron carbide, Al (Aluminum) oxide, and Si carbide, as well as a liquid mediums [3]. USM techniques do not depend on electrical or chemical characteristics of the workpiece material, which makes it capable of machining a wide variety of materials [13–17]. Thus, this technique is commonly used in machining of hard and brittle materials such as Si [18, 19], quartz [20], borosilicate glass [21], titanium alloys [22] and ceramics [23, 24], which are difficult to machine using traditional techniques.

The basic setup for the USM process is presented in Fig. 2a. The configuration consists primarily of a tool system, which uses a transducer to convert electrical energy into mechanical energy, and into an ultrasound frequency vibration tool, with a range of 20 to 40 kHz, and a slurry supply unit [9, 13, 25–27]. Figure 2b shows the material removal mechanism for the USM process. In general, there are four types of material removal mechanisms in the USM operation, namely, mechanical abrasion, microchipping, cavitation effects, and chemical actions. In the mechanical abrasion

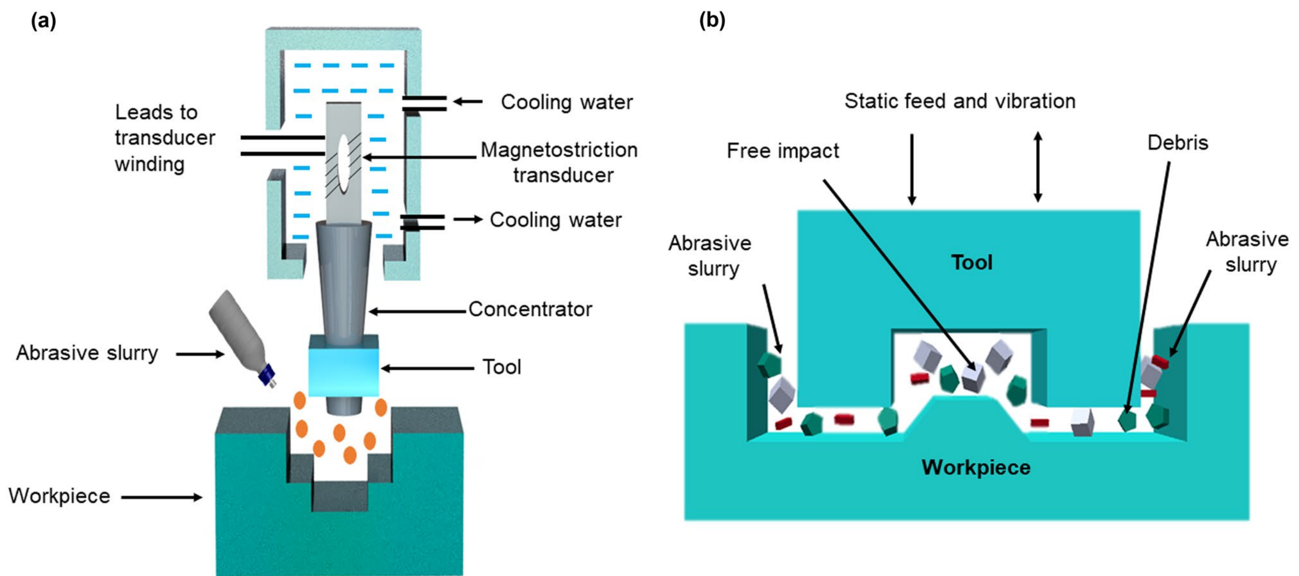

Fig. 2 Ultrasonic machining (**a**) basic setup of the USM and its (**b**) material removal mechanisms. Source: own authors

mechanism, the material removal action is generated by the direct hammering of the abrasive particles against the workpiece surface, to remove small amounts of material [9]. On the other hand, microchipping can be accomplished by vibrating the machine tool, which moves the abrasive slurry freely, and produces an effect on the surface of the workpiece [7, 9]. The material removal process can also be created by the implosion of gas bubbles, known as cavitation effects in liquids, which have been agitated by ultrasonic vibration. The chemical action causes deterioration of the workpiece material due to chemical contaminants in the slurry medium, resulting in material losses [9].

The variants of machine tool motion in USM can be divided into three types, namely, stationary USM, rotary USM, and hybrid USM. The stationary USM principle is based on the idea of micromachining by means of a microtool, that does not require rotary motion [9]. The machining process can be carried out using the vibration of the tool and workpiece. The tool vibrates at small amplitudes, and accelerates the free abrasive particles in the slurry, thus producing momentum and impact on the surface of the workpiece. However, the tool vibrations can cause shortening of the tool length, and difficulties in maintaining the accuracy of the vibration amplitude. The ultrasonic vibration of the workpiece is preferable due to the removal of the vibration amplitude from the tool, and further helps to improve the performance by stirring the abrasive slurry, and removing debris [9, 28]. On the other hand, rotary USM uses a rotating diamond-plated tool to extract the material from the workpiece mechanically. This incorporates both diamond grinding and USM, leading to a higher MRR than individual diamond grinding or USM [24]. Additionally, rotary USM can be further divided into tool and workpiece rotations. However, the rotation of the workpiece is claimed to lead to a better MRR, because of the combined effects of the material removal, due to the sliding form of indentations, scratching of embedded grains, and rolling contact between the abrasive grains on the workpiece [29]. Hybrid USM is a combination of USM with other micromachining methods, such as EDM, electrochemical machining, wire electrical discharge grinding (WEDG), and other non-traditional machining techniques, to address the drawbacks of previous techniques [9]. Hybrid USM, together with EDM and WEDG, enables the manufacturing of 3D microstructures with high aspect ratios [12]. Nevertheless, the combination of the USM with EDM and abrasive flow machining has resulted in improved performances [30].

2.1.1 Ultrasonic machining performances

The USM performance is commonly investigated based on the MRR, tool wear rate, and quality of the machined surface. The desired features of USM consist of an economically viable machine, with the necessary surface topography, while maintaining an excellent finish, minimal damage, high-dimensional accuracy, and a reasonable MRR value. MRR can be expressed in mm3/min, as shown in Eq. (1) [3]:

$$MRR = 5.9F\left(\frac{S}{H_0}\right)R^{0.5}Y^{0.5} \quad (1)$$

where F and S describes the oscillation frequency (Hz), static stress on the tool (kg/mm^2), respectively; H_0, Y, and R defines the surface fracture strength (Brinell hardness

number (BHN)), the vibration amplitude (mm), and mean radius of grit (mm), respectively. Equation 1 indicated that the MRR of the USM dependent on the tool's vibration frequency, the size of the machined area, static pressure, the abrasive used, and the workpiece material [3]. The MRR increases as the amplitude of the tool vibration and abrasive grain size increases, and as the tool to workpiece hardness ratio, and tool area decreases. The large tool size limits the distribution of abrasive slurs over the entire machining area, and affects the MRR [3].

Apart from MRR, the main aspect of USM is tool wear that affects the MRR and machining accuracy. The tool wear ratio can be expressed as the ratio of tool wear length to machining depth. In USM, as harder and coarser abrasive grains are utilized, the wear of the tool appears to increase due to the penetration of the abrasive grains into the tool, resulting in higher MRR of the workpiece [7]. Another important USM performance criteria is the quality of machining of the workpiece material surface finish, which can be measured by three significant criteria, such as the surface roughness, taper ratio and out-of-roundness [11, 12]. The size of the abrasive grains influences the surface roughness, in which smaller size abrasive grains yield smoother surfaces due to smaller crates. When large abrasive particles are utilized, more debris is eliminated from the region where the machine is working, and the abrasive particles can readily move to other places because of vibrations.

2.1.2 Ultrasonic machining on Si wafers

USM has proven its effectiveness in the machining of 3D geometry shapes on the Si wafer, as shown in Fig. 3. For example, Sun et al. [12] proposed the machining of Si wafers using hybrid USM with a combination of WEDG and EDM on USM, as shown in Fig. 3a to fabricate high-aspect-ratio 3D microholes, as small as 15 µm in diameter for sensors fabrication. In order to prove the effectiveness of the USM for Si micromachining, Egashira et al. [31] implemented a 3D triangular hole on Si using the tool fabricated using the WEDG technique, as shown in Fig. 3b. Later, in 1999, Egashira and Masuzawa [28] introduced a sintered diamond (SD) with high wear-resistance as a tool material, to solve the problem of high tool wear for tungsten carbide (WC) alloy tools. The improvement in the tool wear rate contributed to the creation of multiple holes using single tools. As a result, Fig. 3c shows 48 microholes which were fabricated on Si using the SD tool, with an average diameter of 22 µm, and a depth of 10 µm. In 2004, Yu et al. [32] demonstrated 66 µm diameter microholes and 3D microcavity machining using USM on Si wafer. The authors claimed that a smoother surface obtained by reducing the cutting depth of each

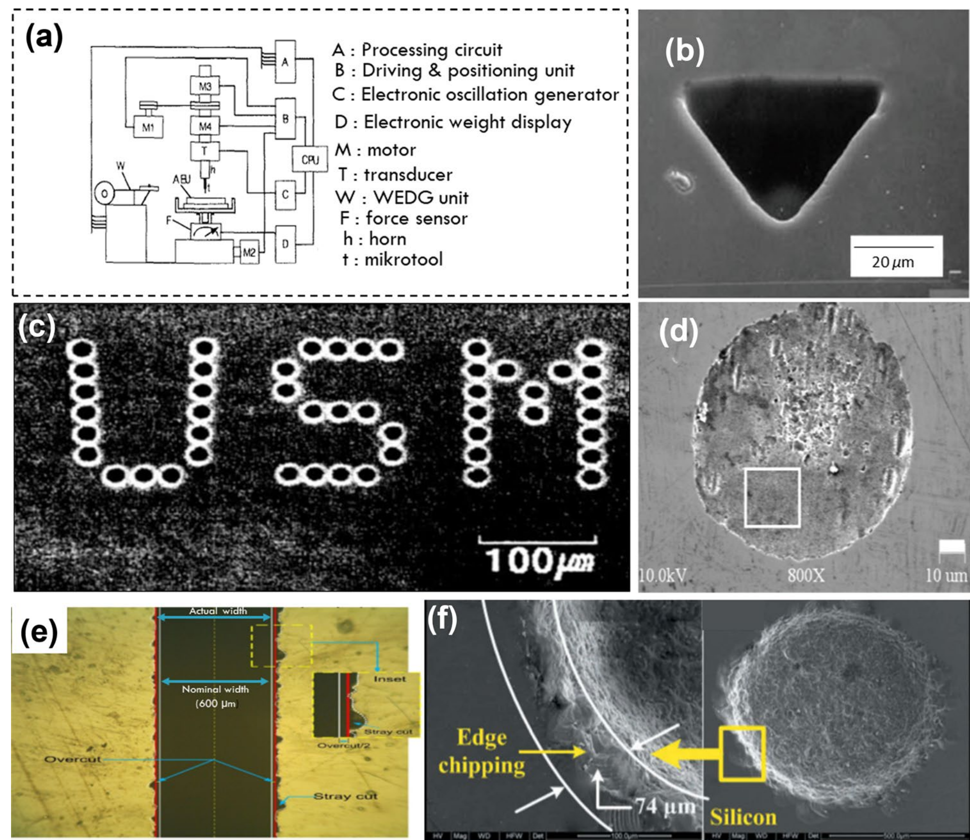

Fig. 3 Machining of the Si wafer by the USM; (**a**) Configuration of micro-USM system. Source: adapted from Sun et al. [12]; (**b**) 3D triangular microhole with WEDG tool. Source: adapted from Egashira et al. [31]; (**c**) 48 microholes by single SD tool. Source: adapted from Egashira and Masuzawa [28]; (**d**) Surface quality of hole without tool rotation. Source: adapted from Yu et al. [18]; (**e**) Top view of a typical microchannel. Source: adapted from Sreehari and Sharma [35]; (**f**) Surface quality and edge chipping of hole periphery. Source: adapted from Kumar and Dvivedi [36]

layer resulted in an improvement in machining time. Later in 2006, Yu et al. [18] explored the effects of machining parameters on USM performances. Figure 3d illustrates the Si machined surface of 0.25 µm without tool rotation, and a higher surface roughness of 533 nm, due to locally concentrated abrasive particles. This result showed that the rotation of the tool on the surface roughness was not important, and that the size of the abrasive particles was found to be the main factor affecting the surface roughness of the USM.

In 2008, Tsui et al. [33] proposed a new PZT actuated ultrasonic workpiece holder, instead of a vibrating drill. The results revealed that this method provides enhanced machining quality, efficiency, and longer life tool for Si wafer machining. Zarepour and Yeo [34] reported on a developed methodology based on single abrasive particles, in order to determine the mode of material removal on Si, ductile, and brittle materials using USM. The brittle and ductile mode of material removal resulted in a single particle size of 0.37 µm, at a vibration amplitude of 3 µm.

Microchannel manufacturing technologies have played an imperative role in the production of bio-MEMS. In 2011, conventional USM was successfully used to developed microchannels on glass and Si, as one of the potential research development areas for USM machining [9]. Cong et al. [19] presented a study on edge chipping in rotary USM of Si, which evaluated the relationship between edge chipping and the cutting force. The results showed that the high speed of the rotation tool, high ultrasonic power, and the low feed rate, contributed to the generation of small edge chipping and low cutting forces, whereby the cutting force was an important parameter which could affect the edge chipping. In 2018, Sreehari and Sharma [35] investigated the improvement in the quality of microchannels (Fig. 3e) fabricated using micro-USM, in terms of surface roughness, over-cutting, and stray cutting. As a result, low viscous fluids and higher feed rates resulted in an enhanced surface finish and accuracy. Over-cutting and stray cutting could be reduced using high viscous fluids.

In 2019, the latest production of micro-USM using rotary tool drilling techniques on micro-holes machining on zirconia, silicon, and glass was been reported by Kumar and Dvivedi [36]. Figure 3f demonstrates different roughness of the machined holes using different tool rotation speeds of 100–700 rpm. The experimental results justified the setting of the upper and lower rotational bounds at 500 and 100 rpm, in order to achieve successive machined surfaces. The study found that the maximum MRR and depth of the micro-holes were generated in the machining of the Si material. The over-cutting aspect was also found to be maximum in Si, relative to two other materials, i.e., zirconia and glass. Table 1 provides a summary of the machining of Si wafers using the USM technique.

2.2 Ion beam machining

IBM, commonly known as ion etching, ion milling, or ion polishing [3] techniques, was introduced in the 1950s, for the preparation of transmission electron microscope (TEM) samples of earth-based mineral specimens [37, 38]. Previously, IBM was introduced for TEM examination of metals and biological tissues, which provided unsatisfactory results when applied to brittle oxides which were comprised of bulk of earth and meteorites. However, throughout extended studies, the findings showed that most minerals could be thinned to electron transparency with an acceptable low level of radiation damage at ~ 6 keV using ion bombardment [39]. The Argon (Ar) ion milling technique covered the standard means for the preparation of TEM mineral specimens [40]. The material removal process occurred with the transfer momentum from incident ions to atoms on the material surface, resulting in the removal of atoms and deflection of ions from the material. The mechanism is inextricably linked to the emission of atoms from the surface by additional ionized atoms (ions) bombarding the working substance [41].

Figure 4 shows an ion milling setup consisting of ion sources that generate sufficiently intense beams with an appropriate spread of energy, to extract atoms from the workpiece via impingement of ions. A cathode, i.e., a heated tungsten (W) filament, accelerates electrons utilizing a high voltage (1 kV) to pass into the anode. The electrons move from the cathode to the anode and contact with Ar atoms in a plasma source to form Ar ions. This forms an electron spiral by inducing a magnetic field between the cathode and the anode. The ions formed are then retrieved from the plasma and transferred to the workpiece, which is positioned on a water-cooled table and tilted at an angle ranging from 0˚ to 180˚ [3].

Focused ion beam (FIB) milling is a technique which is similar to that of IBM, but with a limited machining area [42]. The FIB technique provides many advantages which can overcome the limitations attributed to conventional Ar ion millings, such as the ability to extract a sample from extremely small quantities of unpolished material, site specificity on a sub-micrometer scale, sample imaging of secondary ions or electrons during milling, and rapid processing of super hard materials [39, 43]. FIB is commonly used in the semiconductor field for circuit modification, layout verification, microcircuit failure analysis, and mask repair [44–46]. In addition, TEM specimens of metals, ceramics, semiconductors, and biological materials have also been prepared using the FIB milling technique, by Giannuzzi et al. [47]. Chen and Zhang [48] used the FIB technology to analyze and report on microcircuit failure analysis. This method effectively examined invisible defects in the internal structure.

Table 1 Summary of machined Si wafers using USM

References	Year	Type of USM	Tool properties	Machining settings	MRR	SR	Comments
[12]	1996	HUM	WC alloy	Abrasive: WC, D-0.58 µm Vibration amplitude: 1–3.5 µm Working load: < 0.1mgf/ µm2 Machining speed: 2–6 µm/min	MRR: 1.18 × 10–5 mm3/min	SR: 0.2 µm	-Microholes 15 µm in diameter -3D turbine chamber
[31]	1997	RUM	WC alloy	Abrasive: WC, D-0.58 µm Working load: 1–2 mN Vibration amplitude: 0.8 µm Frequency: 40 kHz	MRR: 1.31 × 10–6 mm3/min	N/A	-Microcavities with sharp corner -Machining microhole: square, triangular, trench
[28]	1999	SUM	WC alloy	Abrasives Diamond: 0.2 µm Vibration amplitude: 0.25 µm Working load: 0.7–10 mN	MRR: 1.73 × 10–6 mm3/min	N/A	Hole: 10 µm depth Tool: 10.5 µm
[32]	2004	RUM	W 50 µm	Tool feed: 143.5 µm Abrasives Polycrystalline diamond powder: 1–3,0.5–1 µm Vibration amplitude: 3 µm, 5 µm Frequency: 39.5 kHz Working load: 10–20 mg Taper Volume: 231 × 231x69µm3 Radius: 50 µm	MRR: 2.6 × 10–3 mm3/min	N/A	-Hole: 66 µm diameter with 200 µm tool feed -3D microcavity: 69 µm depth
[18]	2006	RUM	W 95 µm	Rotational speed: 3000 rpm Abrasives Polycrystalline diamond: 0.25,0.5–1,1-3 µm Vibration amplitude: 1,1.25,1.5 µm Frequency: 39.5 kHz Working load: 1-12 g	MRR: N/A	SR: 0.42 µm	-Machining 3D microholes
[33]	2008	RUM	WC alloy Diameter: 0.605 mm	Rotational speed: 50000 rpm Tool feed: 0.02,0.01, 0.005 mm/min Vibration amplitude:1 µm Frequency:20 kHz	MRR: 5.65 × 10–3 mm3/min	N/A	-Design workpiece holder from medium carbon steel (SAE1045) -Hole: 320 µm depth
[9]	2011	SUM	Stainless steel	Abrasives Si carbide: 20 µm Frequency:20 kHz	MRR: 0.47 mm3/min	N/A	Microchannels

Table 1 (continued)

References	Year	Type of USM	Tool properties	Machining settings	MRR	SR	Comments
[19]	2012	RUM	Metal-bonded diamond Diameter (O): 9.53 mm Diameter (I): 8.0 mm L-45 mm	Rotational speed: 2000-4000 rpm Tool feed rate: 0.01–0.03 mm/s Abrasives Diamond: 89-104 µm Frequency:20 kHz Working load: 7-20 N	MRR: 2.14 mm3/sec	N/A	-Drilling hole with 700 µm -Edge chipping thickness: Highest 0.31 mm -Size of Si: 20 × 20x0.7 mm
[34]	2012	SUM	W Diameter 300 µm	Frequency:50 kHz Amplitude:0.8–5 µm Abrasive particles Polycrystalline diamond: 0.25–4 µm Concentration: 0.02, 0.04 wt%	MRR: N/A	SR: 4.5 µm	-Approached single abrasive particle impingement to study on brittle MR mode in USM
[35]	2018	SUM	WC alloy Diameter 600 µm	Abrasives Silicon carbide: 1800 mesh Slurry medium-palm oil, transformer oil, water Frequency: 20 kHz Power: 800 W	MRR: N/A	SR: 0.35 µm-abrasive concentration 15% SR: 0.4 µm-abrasive concentration 20%	-Design microchannel with Volume: 0.6 × 0.3 × 10 mm3 -Feed rate: 20 mm/min, transformer oil
[36]	2019	RUM	WC alloy	Rotational speed: 100–500 rpm Frequency: 21 kHz Static load: 60 g Abrasive: WC Abrasive sizes: 1000–1800 mesh	MRR: -300 rpm: 0.58 mg/min,	N/A	-Microholes on hard brittle materials

FIB milling has two basic modes; direct-write ion beam, and ion-beam projection. The process which uses direct impingement of the ion beam on the substrate to transfer patterns is called ion beam direct-write. This technique has been successfully used in the manufacturing of 3D microstructures, and devices made of different materials. An ion beam projection, a collimated beam of ions, passes through the stencil mask, and a small image is projected onto the substrate underneath [45]. The working area for FIB is limited to tens of square micrometers [42] and requires a long machining time [49, 50].

2.2.1 Ion beam machining performances

In IBM, as ions strike the workpiece obliquely, the atom ejection mechanism is caused by the collision that creates momentum. The occurrence of momentum depends on whether the energy levels are low or high, when the ions collide. Under these conditions, it is reported that the incident momentum vector has the largest impact on the ejection process. The rate of machining depends on the material, sort of ions, and their energy, as well as on the incidence angle [41]. Equation (2) describes the rate of etch, $V(\theta)$, in [atoms per minute/(mA.cm^{-2})] [41]:

$$V(\theta) = \frac{\left(9.6 \times 10^{25}\right) S(\theta) cos(\theta)}{n} \quad (2)$$

where, $S(\theta)$ and n describe the yield (atoms per ion), and density of the target material (atoms per cm^3), respectively.

The efficiency or etch rate, depends on the FIB process parameters, such as ion beam current, extraction voltage, angle of incidence, milling time, dwell time, and percentage overlap between beam diameters. Among these process parameters, ion beam current has the most important control of the MRR and SR for the FIB performance, as stated by Bhavsar et al. [51]. Tang et al. [52] reported that an applied lower operating voltage was one of the solutions to minimize ion beam damage in the TEM specimen preparation. Dwell time, which is the duration of time the ion beam remains fixed at one-pixel point [53], increased the dwell time, which resulted in a high SR [54].

In terms of accuracy, the dimension scale can be as small as 10 to 100 nm [3]. The surface finish in ion milling is defined by the incidence angle of the ion beam. McGeough

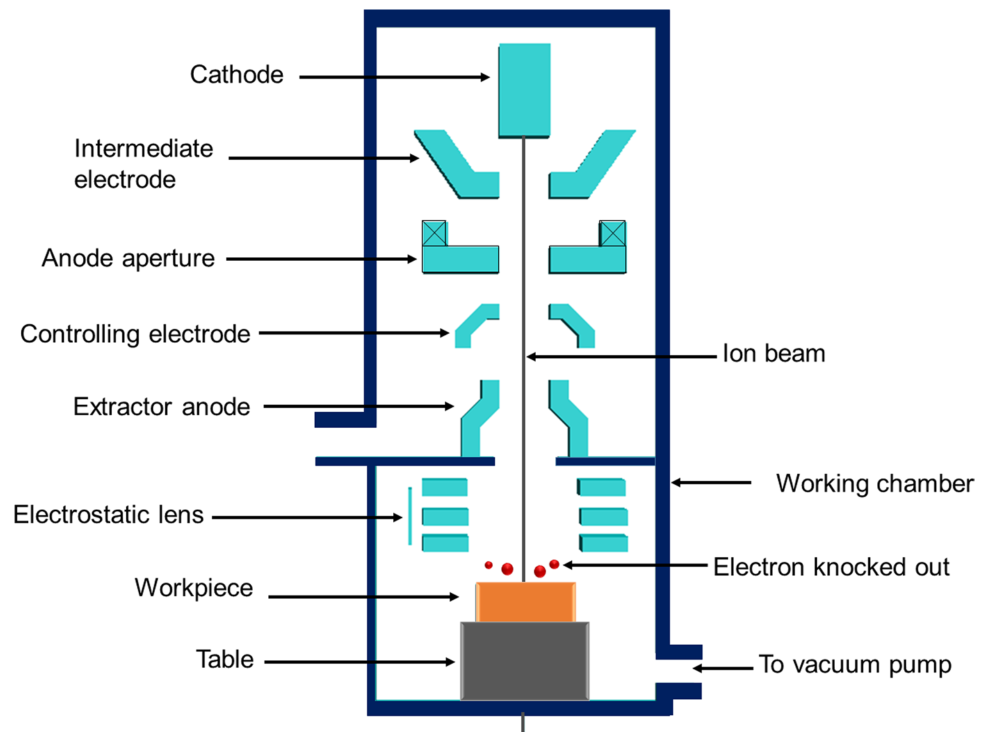

Fig. 4 Schematic diagram of ion beam milling system. Source: own authors

[41] reported that they achieved an accuracy level of 1.0%, with a repeatability of ± 1%. The FIB machining method can accomplished a surface with a feature size at, or below 1 µm, with a very short wavelength, and a very large density [45].

2.2.2 Ion beam machining on Si wafers

The Ar ion milling for the preparation of TEM specimens for compound semiconductors may generate serious artefacts, including metallic surfaces islands, small crystallographic defects, and near-surface cavities. Chew and Cullis [55] studied the performance of ion milling when using various ion species, and different machining conditions. The study showed that there had been an improvement in the quality of the specimens when a suitable selection of ion species and ion milling conditions were combined. Compared to traditional Ar ion milling, the FIB technique offers a range of capabilities for providing a fast method for preparing TEM specimens, and sequential cross-sectioning of multi-level layers from several types of materials, so that preferential sputtering can be neglected [56]. Hung et al. [46] looked into the characterization and optimization of the operating parameters which affect the FIB milling system using the Ga + ion process on a Si wafer as shown in Fig. 5a. The parameters affected the machining performance, which was the studied MRR and surface integrity values.

In 2007, Hopman et al. [57] investigated the FIB fabrication of submicrometer holes with improved vertical sidewalls, using raster and spiral scan routines as sidewall optimization parameters on various materials, such as Si, Si-on-insulator and Si membranes. Different cross-sectioning methods have been used to examine the effects of milling parameters towards the geometries of submicrometer-sized holes, which include milling with a sloped milling depth, line by line polishing, and combinations for both methods. In 2009, Amirmajdi et al. [42] developed a MEMS device on a Si membrane using the ion beam method, with a 5 kV beam. The cross-section of MEMS devices can only be prepared using the ion beam method, because the mechanical polishing technique can't handle the brittle nature of Si. To study the minimization of the surface damage during TEM sample preparation, Pastewka et al. [44] proposed low beam energies for FIB polishing. The authors prepared TEM samples with amorphous layers, using 2 and 5 kV beams for polishing, which was able to determine the 1.4 and 4.6 nm thickness, respectively. Figure 5b shows the high-resolution TEM images of the interface of amorphous layers between a platinum (Pt)-coating and Si, with 2 kV polishing beams. The overall results showed that the thickness of the amorphous layers were linearly dependent on the beam energy, of which high beam energy led to low quality surfaces. In 2010, Tang et al. [52] machined three different materials, Si, Zinc (Zn) oxide, and Copper (Cu), on normal and low voltage FIB ion beam damages for TEM sample preparation. The FIB-preparation method for TEM specimens have been extensively investigated and compared. Low voltage FIB has been identified as one of the solutions to reduce ion beam damage of materials.

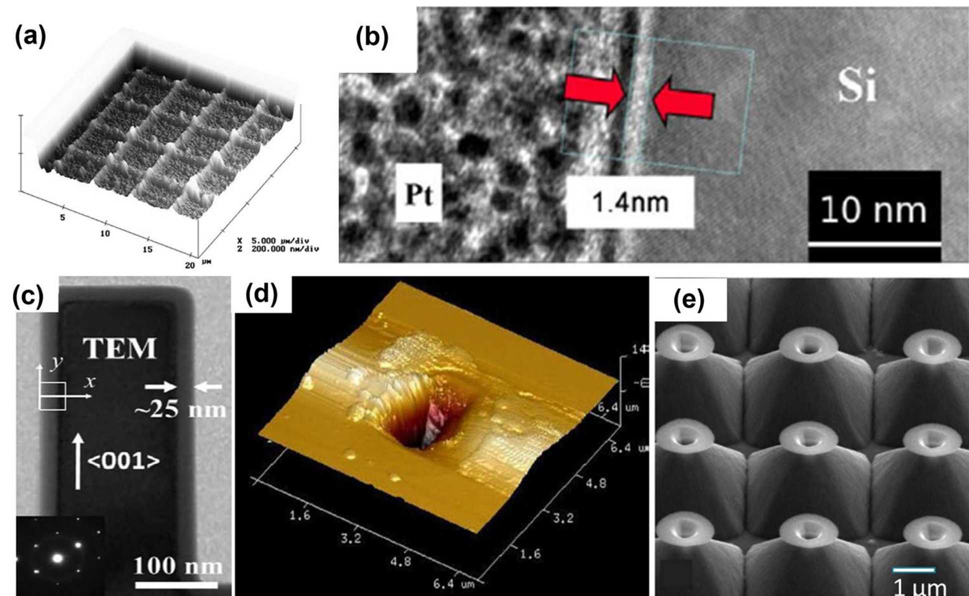

Fig. 5 Si machining by IBM techniques (**a**) The grit lines. Source: adapted from Hung et al. [46]; (**b**) TEM image of Pt-coating and Si. Source: adapted from Pastewka et al. [44]; (**c**) TEM image of FIB milled on Si pillar. Source: adapted from Salvati et al. [59]; (**d**) AFM image of holed milled at 1nA current in Si. Source: adapted from Goswami et al. [60]; (**e**) SEM image of 3D engineered nanotrumpets. Source: adapted from Garg et al. [61]

In 2014, Sabouri et al. [58] also investigated the subsurface damage of Si, along with the effect of dwell time on Ga + FIB machining operations. The analyzed results showed that higher dwell times reduced the surface damage of Si as the dwell time increased due to the catalyst activity of Ga inside Si, which helps to reduce the activation energy for crystallization. In 2018, Salvati et al. [59] studied nanoscale Si structural damage due to FIB with Ga + ions, as shown in Fig. 5c.

Apart from cross-sectioning purposes, the FIB technique for the machining of 3D micro-nanostructures such as nanomoulds, nanomesh, pyramids, nanotrumpets over pyramid arrays, have been demonstrated. In 2017, Goswami et al. [60] approached micro/nanoscale structures for machining Si to fabricate nanomoulds. Trials were conducted at different levels of beam currents and severe damage was observed when 1 nA current applied as shown in Fig. 5d. The process parameters for FIB such as beam current, dwell time, and percentage overlap, were optimized to maximize MRR and minimize SR of the milled cavities. In 2020, Garg et al. [61] successfully fabricated various Si 3D micro-nanostructures using the Ga-FIB technique, by combining ion implantation and selective chemical etching. Figure 5e displays the SEM images of engineered 3D nanotrumpets for antireflection and color filtering applications. In conclusion, the ability to fabricate 3D micro-nanostructures using ion implantation and chemical etching offers a new route towards 3D nanofabrication for developing unique structures on Si. Table 2 provides a summary of Si wafers machined using the IBM technique.

2.3 Laser beam machining

The ability of LBM to machine submicron structures in various materials such as metals, semiconductors and ceramics including silver, Cu, brass and stainless steel, has attracted researchers to explore this method of machining much further. It has been widely used in many industrial applications, including plating, heat treatment, cladding, alloying, welding, and machining [3, 62, 63]. Einstein was the first to introduce the concept of stimulated emissions in the theory of lasers [64]. In 1957, Townes and Shawlow invented the first laser called the Ruby Laser [65]. The term "Laser" is an abbreviation for Light Amplification by Stimulating Radiation Emission, which is a strongly collimated, monochromatic, coherent and amplified electromagnetic beam, focused on a small area [3, 66]. The light amplification is the main component of the laser beam, which is accomplished by stimulating the release of high-energy incident photons. Lasers consist of three significant components; a lasing medium, a lasing energy source that stimulates the lasing medium to its amplifying state, and an optical feedback system. The laser medium may be divided into solid (neodymium-doped yttrium-Al-garnet (Nd: YAG)), liquid (dye), and gases consisting of carbon dioxide (CO2), helium (He), Ar, and neon. The laser beam has photons of same frequency, wavelength, and phase, that differentiate it from ordinary light [66]. These features make the LBM unique, such as high directionality, high power density, and enhanced focus [66].

There are generally three main types of LBM techniques; Nd: YAG, CO2 and excimer laser [67, 68]. The Nd: YAG

Table 2 Summary of machined Si wafers using IBM

References	Year	Type of IBM	Ion beam properties	Machining settings	MRR	SR	Comments
[55]	1987	Ion beam thinning Ar ion milling	Ar ion beam milling	Energy: 2.5–7.5 keV	N/A	N/A	-Fabrication of high-quality specimens- using I + ion milling -Roughness of I + increase than Ar +
[56]	1998	FIB thinning	FIB lift-out	-Voltage: 300 kV for 3–5 h -Thinning layer: ~ 100 µm	N/A	N/A	-Develop fast technique in preparation of TEM specimens
[46]	2002	FIB Gallium	Dual FIB using e-/ Ga + ions	Pixel spacing: 0.01 µm -Dwell time: 10 µs	MRR: 3.4 mm3/sec	SR: 2–5 nm	-Optimize parameter affect FIB milling on Si -0.8 µm3/s - measured -1.1 µm3/s–predicted
[57]	2007	FIB Gallium liquid metal sources	Dual-beam FIB contains ion and electron beam	-Deposit: Pt layer -Dwell time: 0.1 ms -Current: 48 pA -Sputter rate: 0.27 µm3 nC-1 at 30 kV -Dose: 69 pC	N/A	N/A	-Optimization parameter with references to sidewall angle -Single hole and patterns milled for 12 and 36 array –array holes higher than single hole
[42]	2009	Ion milling Ar	Ar ion beam milling	-Voltage: 5 kV for 10 h -Diameter: 5 µm -Depth: 10 µm	N/A	N/A	-Fabricate 3D Si detector
[44]	2009	FIB	Ga ions	-Voltage: 2 keV -Current: 500 pA -Polished with 2 and 5 kV -Deposit: Pt-coating	MRR: 1.14 nm3/impact	N/A	-Fabricate trench with low beam energies -Thickness of amorphous layer: 1.4 nm (2 kV)
[52]	2010	FIB	Ga ion	-Voltage: 30 kV, 2 kV -Thickness: 500 and 300 nm -Current: 590 and 83pA	N/A	N/A	-Fabricate trenches with two beam voltage -Thickness of amorphous layer: -2 nm (2 kV) -24 nm (30 kV)
[58]	2014	FIB	-Ga ion -Pressure: 10–6 mbar	-Energy: 30 keV -Pixel dwell time: 0.1, 1, 1.0 µs -Dose: 1018 ions/cm2 Currents: 100, 300, 500, 1000pA	N/A	N/A	-Effect of dwell time on Si at different currents -Study on changing pixel dwell time towards
[60]	2017	FIB	Dual beam	Current: 10, 30, 50 pA Dwell time: 1, 4, 7 µs Percentage overlap: 25, 50, 75%	MRR: 7.414 × 10–3 µm3/s	SR: 1.93 nm (exp) 1.89 nm (model)	-Fabricate nanonoulds from micro/nano machining Si -7.414 × 10–3 µm3/s

Table 2 (continued)

References	Year	Type of IBM	Ion beam properties	Machining settings	MRR	SR	Comments
[59]	2018	FIB	-Ga ions -Beam size width-0.5 mm height-0.2 mm	-Energy: 30 keV -Current: 0.3 nA -Dose: 2.0 × 109 ions/μm2	N/A	N/A	-Characterize ion beam damage by X-ray technique -Thickness of amorphous layer: 23 nm
[61]	2020	FIB	Ga ion	-Voltage: 30 kV -Currents: 10 pA -Dose: 1 × 1012 – 5 × 1016 ions/cm2	N/A	SR: 0.4 nm	-Fabricate 3D Si micro-nanostructures with FIB and followed by wet chemical etching, KOH -Thickness of implantation damage: 20 nm

laser uses a solid laser material as a medium, which can be used for high-power boring and engraving purposes. It has a low beam power however, high peak powers can be reached when the laser is operated in a pulsed mode, making it possible to machine thick materials. In addition, this type of laser technique allows the machining of thin materials with a shorter pulse duration [69]. On the other hand, the CO2 laser is dependent on the discharge of a gas chamber filled with CO2, hydrogen, nitrogen, and He. The CO2 laser wavelength is 10 μm within the infrared region and has a low-resolution machining. However, it has a relatively high beam power, improved efficiency, and superior beam quality, making it appropriate for high-speed metal cutting [70]. Apart from these techniques, the excimer laser is generated from a compound of two identical species in an exciting state [65, 71]. The excimer lasers are pulsed lasers that operate in ultraviolet mode, by rapid electrical discharge under high-pressure mixtures of rare gases, such as krypton, Ar, or xenon, as well as halogen gases such as fluorine, or hydrogen chloride [69]. The mixture of rare gases and halogen produces varying output wavelengths, ranging from 0.193–0.351 μm in ultraviolet (UV) to near-UV spectrum [65]. The pulse energies form a few hundred millijoules to one joule, and the average power is between 10 W and 1 kW. The pulse length is normally in the range of 10–20 ns, generating a peak power of tens of megawatts [69]. The excimer laser is commonly used for the machining of solid polymer workpieces, ceramics and semiconductors, and marking of thermally sensitive materials [65].

The LBM consists of laser optics and a computer numerical control (CNC) operated stage. The CNC cutting process allows the system to create designs for the workpiece, with the desired patterns. Figure 6a shows the configuration and physical operation of the LBM system. LBM is a thermal process whose performance is determined by the amount of heat produced as well as the optical properties of the materials, instead of their mechanical properties [66]. The physics of the LBM process is very complex due to the loss of scattering and reflection on the machined surface [72]. Figure 6b shows that the LBM material removal process consists of three stages: absorption and heating, melting, vaporization, and chemical degradation [66]. The process begins when the high energy density of the laser beam is focused on the surface of the workpiece. The absorbed thermal energy heats and changes the workpiece material into a molten or vaporized state. These molten materials are removed using a flow of high-pressure gas jet that helps to accelerate changes in the material, and ejects it from the machining zone [66]. The removal mechanism depends on the power density, and the pulse time of the laser beam [3]. There are three ablation parameters for the pulse duration in LBM, namely, nanosecond, picosecond and femtosecond [73]. In comparison, the nanosecond laser has a shorter wavelength and a higher pulse duration than the femtosecond ablation. The picosecond laser pulses are shorter, while the femtosecond laser is ultra-short, which categorizes it an infrared laser with a wavelength of approximately 1053 nm [74]. The femtosecond laser uses a unique ultra-short laser pulse ablation to achieve a high degree of control when sculpting the targeted microstructures without causing collateral damage, making it suitable for thin wafer dicing due to its superior machining quality [75]. Thus, the femtosecond laser has advantages over the nanosecond laser because it promises the ability to create a smaller and more precise hole, with a lower pulse energy and a lower repetition rate [76].

In LBM, thermal damage of the base material due to excessive heat during machining remains a major problem

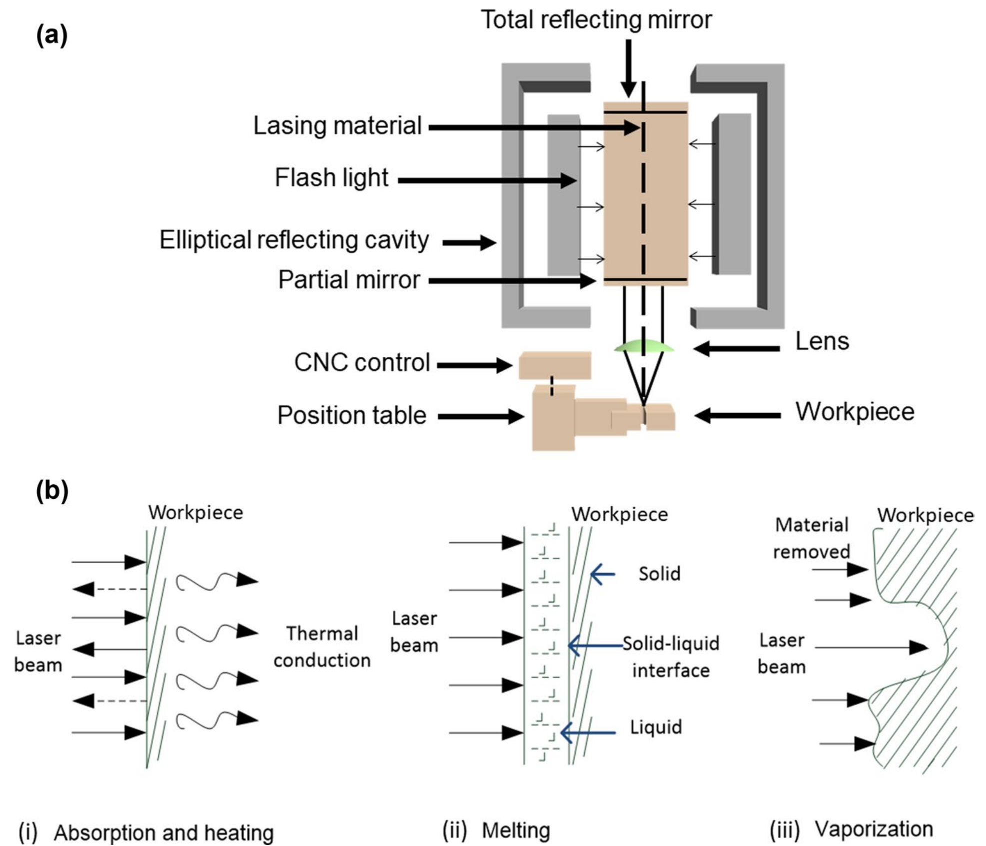

Fig. 6 (**a**) LBM system and (**b**) Material removal mechanism of LBM. Source: own authors

for nanosecond lasers, that needs to be minimized to achieve a high surface-machining quality [77]. The thermal damage area is also associated with undesirable side effects, such as distortion, surface cracking, embrittlement, decreased weldability, fatigue resistance, and increased corrosion [78]. It is vital to precisely quantify the relationship between the magnitude of thermal damage and the cutting conditions, in order to minimize the thermal damage for nanosecond machining. Nevertheless, due to the extremely short laser pulse width, there is almost no time for the propagation of heat to the surrounding area, which is often referred to as a nonthermal process. The ultrashort pulse width restrains the formation of thermal damage in the femtosecond laser [79].

2.3.1 Laser beam machining performances

Numerous process parameters can affect the performance of LBM, including the laser power type, the assist gas pressure, the thickness of the cutting material, the material composition, the cutting speed, and the mode of operation (continuous or pulsed mode) [66]. Theoretically, the material is removed by several reactions involving the reflection, absorption and conduction effects of light, melting and evaporation. The MRR performances were generated from the workpiece material in response to these reactions. The reflection effects depend on wavelength, material properties, surface finish, oxidation levels and temperature. The higher reflection of the workpiece material at a specific wavelength resulted in lower MRR [3]. There are several experimental studies on MRR, which have been reported. Voisey et al. [80] showed that the MRR increased when the pulse energy increased. Tahmouch et al. [81] revealed that higher power and lower frequencies resulted in higher MRR. Chen and Darling [82] showed that the MRR increased when the beam energy density increased, irrespective of the machining speed. Equation (3) represents the MRR (mm^3/min) of LBM as [3]:

$$MRR = \frac{4C_l L_p}{\pi E_v (F_l \alpha)^2 h} \tag{3}$$

where, C_l is a constant, based on the material and conversion efficiencies; L_p, E_v, F_l, α and h define the laser power (Watt), vaporization energy of the material (W/mm^3), the focal length of the lens (cm), beam divergence (rad), and thickness of the material (mm), respectively.

SR is one of the essential parameters which represents the quality of the machined surface. Experimental studies by Ghani and Newishy [83] revealed that the SR value decreased with increasing machining speed and frequency and decreasing laser power and gas pressure. Chen [84]

showed that the SR decreased when the pressure increased for nitrogen and Ar. The SR was better at higher speeds. The SR was found to be very low, and the laser power had a minimal effect on the SR without affecting the striation frequency.

2.3.2 Laser beam machining on Si wafers

Kruger and Kautek [85] reported on a femtosecond pulse laser at 615 nm, that allowed the creation of a precise microstructure of metallic and semiconductor thin films, without causing material delamination. The femtosecond laser showed sharply defined patterns that could be ablated by the machining of metal plates and Si, compared to the picosecond and nanosecond pulses [86]. Mullernborn et al. [87] demonstrated that fast micromachining of 3D Si can be achieved by direct laser etching (Fig. 7a) using localized melting in an atmosphere with chlorine. The effect of Si surface morphology (100 and 111) which was ablated by the femtosecond pulse laser with different laser parameters, laser fluence, and laser pulse number, was also investigated by Geng et al. [88]. In 2008, Venkatakkrishnan et al. [75] studied the high-repetition-rate of the femtosecond laser for dicing thin Si wafers.

The LBM technique has been applied in the fabrication process of 3D complex structures on Si. In 1999, MEMS devices were fabricated from bulk Si wafers and Si membrane structures using Q-switched Nd: YAG laser technology, with optional frequency doubling, as shown in Fig. 7b [89]. The developed Nd: YAG laser was able to create fast and flexible design modifications. Amer et al. [90] machined optical micrograph of grooves in hexagonal pattern arrays on p-type Si wafers using the excimer laser technique, as shown in Fig. 7c. The grooves of the hexagonal array were 7 mm wide. In 2005, Pan et al. [91] fabricated an arbitrary-shaped microstructure using a dual-prism optical system with a feature size of less than 50 µm, having an aspect ratio of up to 10 µm, which can be reached using UV Nd: YAG lasers, as shown in (Fig. 7d).

There have been several investigations on the effect of process parameters for the LBM method. The analysis of induced stress and amorphization were compared between femtosecond and nanosecond pulses by Amer et al. [77] as shown in Fig. 7e. The results showed that femtosecond pulses produce less stress than nanosecond pulses, and the circular polarized femtosecond lasers had less stress than the linearly polarized laser. Tang et al. [92] studied the kerf width and cut quality effects towards the surface quality. The impact of various processing parameters such as pulse repetition rate, feed rate, pump energy, and the number of passes were optimized to minimize HAZ and achieve the best cutting efficiency. Oxygen gas was found to be the most suitable gas for assisting laser dicing. The highest gas pressure may not yield the best cut quality. Kagerer et al. [93] also investigated parameters such as the number of scans, manufacturing time, input and output diameters, the corresponding flank angle, and the laser micro-cutting holes in Si wafers using nanosecond Nd: YAG UV lasers.

The CO2 and fiber lasers are both rare types of lasers that have been used in Si machining. Chung et al. [94] first demonstrated a novel Si micromachining method using CO2

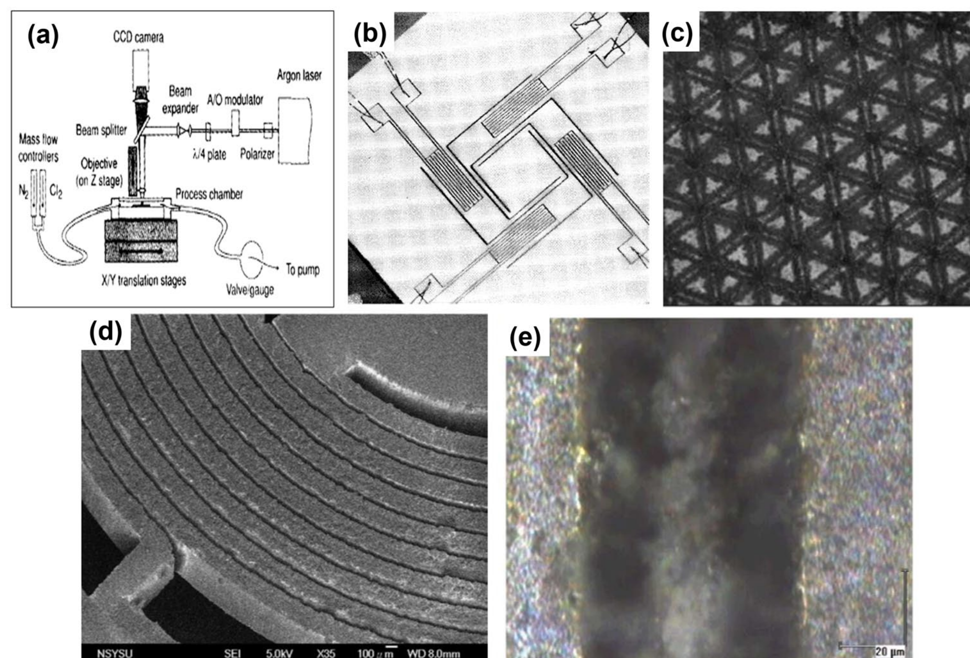

Fig. 7 LBM on Si wafer (**a**) Laser micromachining setup. Source: adapted from Mullernborn et al. [87]; (**b**) Microactuator fabricated by Nd: YAG laser. Source: adapted from Dauer et al. [89]; (**c**) Hexagonal pattern grooves by excimer laser. Source: adapted from Amer et al. [90]; (**d**) Spiral microstructure by UV Nd: YAG. Source: adapted from Pan et al. [91]; (**e**) Machined groove by YVO4 laser. Source: adapted from Amer et al. [77]

lasers in 2006. The experimental results proposed a possible technique for CO2 laser micromachining of Si on glass, using laser absorption variations, because the wavelength of the CO2 laser was not absorbed by the Si. In 2014, Weinhold et al. [95] reported a new method for the fast laser-induced separation of Si wafer materials. This method allowed the possibility to cut monocrystalline and polycrystalline Si wafers in a very fast and clean way, without any waste product.

Several papers have reviewed laser ablation. Wang et al. [96] reported on the investigation of the image processing of the plasma spot produced by femtosecond ablation. The results indicated that the plasma image brightness and picture were affected by the machining parameters. Goodarzi and Hajiesmaeilbaigi [97] investigated the formation of ripple size on the Si surface due to the laser ablation in 2018, across two different environments, air and water. The results revealed that the radiation pressure caused the occurrence of circular ripples to the surface at the end of the pulses. A new physical model using a linearly polarized single femtosecond laser pulse was proposed, which can predict the size and period of the circular ripples.

The machining rate was derived from the performance determined by the machining efficiency. The position of the laser beam must be precisely controlled to achieve optimum efficiency in LBM. Chen et al. [98] have demonstrated a new high-throughput micro-machining of the Nd:YVO4 laser, based on a rapid scanning laser focal point along the optical axis, using an acoustically driven variable focal length lens. The experimental results indicated that the machining rate was more than doubled after the ultrafast z-scanner was applied. The research progress in the machining of Si wafers via LBM is shown in Table 3.

2.4 Electrical discharge machining

EDM uses an electrical discharge or spark, at the gap between the machining tool and the workpiece [99]. Machining Si using EDM has a strong potential for application in the semiconductor industry. EDM is divided into several categories, namely, Die-Sinking and Wire-EDM. Die-sinking EDM was developed in 1940 using pulse generators, planetary, orbital motion techniques, CNC, and adaptive control systems. Extensive research on EDM was performed in 1960, and it focused on various issues related to mathematical modeling. The evolution of wire-EDM began in the 1970s with the development of high-performance generators, novel wire tool electrodes, as well as enhanced machine intelligence and material flushing. Since the 1980s, EDM has been proven as an efficient method for processing hard and brittle conductive materials, including composites and ceramics [100, 101]. EDM is regarded as a non-traditional machining process which is capable of machining complex geometries, regardless of the hardness of work material. However, it is only applicable for machining conductive materials [102–105].

The EDM system consists of two main components: the machine tool and part, as shown in Fig. 8. The machine typically moves in three axes; x, y and z, and an advanced configuration enables the machining of the four axes. Generally, the tool and workpiece are connected to positive and negative terminals, respectively. The machining is conducted in a dielectric fluid that flushes the eroded particles away. The dielectric fluid provides electrical insulation between the electrode and the workpiece, and also functions as a coolant to minimize the heat from the spark. The electrical discharge or the sparks generated at the gap removes the material via the melting and evaporation processes. The MRR of EDM depends on the energy and number of sparks produced by the generator. The higher the energy and number of sparks, the higher the MRR. Each discharge leaves small craters on both the electrode and workpiece. In this process, the speed of the cutting process is regulated by the CNC, which can yield reliable structural results. To achieve high precision machining, the operation and tool conditions must be taken into account in the EDM. High melting and boiling points, high electrical and thermal conductivity, structural integrity (ability to perform its duty without failure), mechanical properties, manufacturability, and cost, are the primary characteristics of the EDM tool selection [106]. Cu, graphite, W and WC are materials most used for EDM tools [107]. Graphite and Cu are widely used as tools due to high electrical and conductive properties. Additionally, graphite offers machinability characteristics, whereas Cu provides good structural integrity [108, 109]. Tungsten has a high melting point and tensile strength, which makes it a highly preferred tool material for EDM [110]. Brass material for tool electrodes can produce stable discharge conditions and is typically utilized for particular applications, such as through hole drilling, where significant tool wear is tolerated [111]. Electrode tool wear in EDM depends on machining energy and polarity, but most importantly, the tool's material melting point plays a crucial role in the EDM tool's wear [112]. Low melting point materials cause high tool wear rates. Furthermore, the change in tool shape caused by electrode wear throughout machining procedures influences the contour of the workpiece, resulting in an inaccurate dimension. The spark gap (the space between the tool and the workpiece) must be regulated during the EDM machining process to avoid short and open circuits. Normally, the gap remains to be few microns for good machining performance. Unstable or non-uniform discharge processes can also occur due to the presence of leftover debris on the workpiece surface and causes short circuit.

As mentioned before, EDM can generally be categorized into two major types; die-sinking and wire-EDM, as shown

Table 3 Summary of machined Si wafers using LBM

References	Year	Type of laser	Machining settings	MRR	SR	Comments
[85]	1995	Excimer	Wavelength: 615 nm Duration pulse: 300 fs Focus distance: 58 mm Ablation threshold: 0.2 J/cm2 Fluence: 2 J/cm2	2.6895 mm3/min	N/A	-Fabricated microstructure Si thin films using femtosecond laser - Velocity: 106 cm/s
[86]	1996	Femtosecond Ti: Sapphire	Laser pulses: 780 nm Pulse energy: 100 mJ Pulse duration: 200 fs to 400 ps No. Of pulses: 0.2–5000 ps Beam diameter: 20 mm Threshold fluence: 2.5 J/cm2 Fluence: 3.7 J/cm2	36.2147 mm3/min	N/A	-Studied on laser ablation by Ti: Sapphire laser pulse
[87]	1996	Excimer Ar ion laser	Focus spot: 1 µm Wavelength: 800 nm Power: 600mW of 488 nm light Etch rate: 105 µm3/s	N/A	N/A	-Fabricated 3D structures by fast laser direct etching
[89]	1999	Q-switched Nd: YAG	Wavelength:1064 nm Frequency: 3 kHz Average power: 4.58 W	N/A	N/A	-Fabricated MEMS devices: Square-shaped microactuator-150 µm × 15 µm length on 380 µm thickness Si
[90]	2002	excimer	Wavelength: 248 nm Duration pulse: 30 µJ per pulse at 100 pulses per second	N/A	SR: 60–100 nm	-Fabricated grooves in hexagonal patterns array with ~ 7 µm wide -Investigate stresses and structural changes in Si wafers
[91]	2005	UV Nd: YAG	Wavelength: 355 nm	N/A	SR: < 50 µm	-Fabricated Si-based spiral microstructures - Holder mover velocity: 2-5 mm/s
[77]	2005	Nd: YVO4 Solid state laser: Nanosecond Femtosecond	-Penetration depth: 770 nm -Nanosecond: Wavelength: 355 nm Pulse duration: 30–50 ns Focus spot: 13 µm Threshold fluence: 44 J/cm2 Fluence: 50 J/cm2 -Femtosecond: Wavelength: 775 nm Pulse duration: 150 fs Focus spot: 50 µm Pulse energy: 17.5 – 950 µJ -Repetition rate:1 kHz Threshold fluence: 8 J/cm2 Fluence: 25 J/cm2	MRR: -Ns: 1.3269 x 10–4 mm3/min -Fs: 2.4643 x 10–5 mm3/min	N/A	-Compared micromachining Si wafer results between 150-femtosecond and 30-ns lasers -Amorphization induced around ± 20 5%
[94]	2006	CO2	Wavelength:10.64 nm Power: 30 W Speed: 1143 mm/sec	N/A	N/A	-Generate circular and linear patterns on Si using CO2 laser - Roughness larger–high pass number

Table 3 (continued)

References	Year	Type of laser	Machining settings	MRR	SR	Comments
[88]	2007	Femtosecond	Wavelength: 775 nm Duration pulse:150 fs Pulse power: 1.1 W Penetration depth: Si (100)–0.001 mm Si (111)–0.00714 mm Laser fluence: Si (100)–0.33 J/cm2 Si (111)–0.30 J/cm2 Threshold fluence: Si (100)–0.08 J/cm2 Si (111)–0.129 J/cm2 Repetition rate: 1 kHz	MRR: -Si (111): 4.8332 x 10–4 mm3/min -Si (100): 1.9084 x 10–4 mm3/min	N/A	-Investigate surface morphology Si (100) and (111) with different laser parameters: Laser fluence and number of laser pulses -Average ripple depth: 1 µm
[75]	2008	-Diode-pumped, Yb-doped -Femtosecond	Wavelength:1030 nm Power: 11 W Frequency: 200 kHz, 26 MHz	N/A	N/A	-Investigate on thin Si wafer dicing by high-repetition-rate femtosecond laser - Kerf width: 16.5 µm -Speed 40 mm/s
[93]	2011	Nd: YAG UV nanosecond	n-type Si wafer thickness of 300 µm	N/A	N/A	-Investigate on laser cutting of microholes in Si -Determine basic parameters in micro-cutting -Highest MRR: 5 µm/scan Gap depth/scan: New-6,7 µm/scan Old-5 µm/scan Machining time: New-73 s, Old-106 s
[95]	2014	Fiber laser: Single mode continuous wave	Wavelength: 1070 nm Beam diameter: 0.75–3.0 mm Power: 150, 3000 W Cutting speed: 1, 2.5, 0.7–15 m/s	N/A	SR: 2 µm, < 4 µm	-Develop very fast laser cutting on Si wafer and generated high surface quality -Maximum cutting speed: 15 m/s
[96]	2017	Femtosecond	Power: 10–50 mW Feed rate: 2–6 µm Speed: 0.4–2 mm/s Energy: > 1 mJ Wavelength: 800 nm Frequency: 1 kHz	N/A	N/A	-Analyze relationship between micromachining processing parameters and image features –Low machining efficiency -Poor machining accuracy
[97]	2018	Ti: sapphire Femtosecond	Wavelength: 790 nm Repetition rate: 10 Hz	MRR: 6.7104 x 10–5 mm3/min	N/A	-Investigate on circular ripple formation in air and water - Circular ripple: Air-1.2 µm Water-0.13 µm
[98]	2018	Nd: YVO4	Wavelength: 355 nm Pulse duration: 15 ns Oscillation Frequency: 140 kHz	MRR: 9.04 × 108 mm3/pulse	N/A	-Demonstrate new high-efficiency laser using ultrafast z-scanner

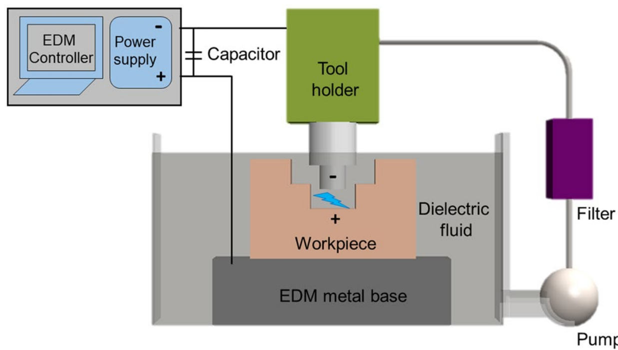

Fig. 8 Schematic diagram of EDM system setup. Source: own authors

in Fig. 9. Die-sinking is also known as conventional EDM, or vertical EDM. Die-sinking EDM can generate blind or through cavities, that are difficult to be formed using conventional machining techniques. Conversely, wire-EDM uses a thin conductive wire as an electrode to cut the material. It is primarily used to cut shapes through the material, given that an initial hole is drilled through the material before the wire is inserted. Compared to the usage of a complex electrode for die-sinking EDM, the wire electrode of the wire-EDM is much more economical for larger shapes, and cut-through applications [113].

2.4.1 Electrical discharge machining performances

The efficiency of the EDM and WIRE-EDM machining processes is determined by process factors such as pulse duration, as well as by discharge frequency and current intensity. Luo [114] discovered that additional high-energy is required to sustain the high MRR without damaging the wire. Suzika and Kishi [115] revealed that lower discharge energy (DE) results in superior surface roughness. The MRR of the EDM is affected by workpiece material, tool electrode material, and machining variables like pulse conditions, machining medium, and electrode polarity. Typically, low melting point workpieces have a higher MRR and surface roughness. Equation (4) represents the MRR in mm^3/min, which was defined by Kalpakjian [116]:

$$MRR = \left(4 \times 10^4\right) i {T_w}^{-1.23} \tag{4}$$

where, i defines the EDM current (A), and T_w is the melting point of the workpiece material (˚C). Based on the material's mechanical properties and the machining conditions, a variety of overlapping crates are generated on the machined surface by the impact of microsecond-duration spark discharges in this process. The impact of discharges per second causes the workpiece to be removed at a specific pace and with a specific surface finish, also with a crater depth reflecting the surface roughness. Since roughness of the machined surface is created by overlapping of craters, the surface roughness increases with the enhance of the MRR.

2.4.2 Electrical discharge machining on Si wafers

The EDM method is a proven method to machine Si wafers with very complex features and shapes, with many useful applications in MEMS. Luo et al. [117] first introduced the Wire-EDM technique as a new Si ingot slicing method, that gives 1.62 μm of surface roughness, instead of using an inner-diameter blade, and a conventional slicing method which has been used before. Uno et al. [118] proved the possibility of slicing Si ingots using a similar Wire-EDM setup. In addition, the experimental results characterized that higher removal rates and smaller SR can be achieved under larger discharge currents and a short pulse duration. Peng and Liao [119] revealed that stable slicing of Si ingot was achieved using the Wire-EDM with water flushing under small currents and lower gap voltage conditions (Fig. 10a). Although the Wire-EDM enables the slicing of

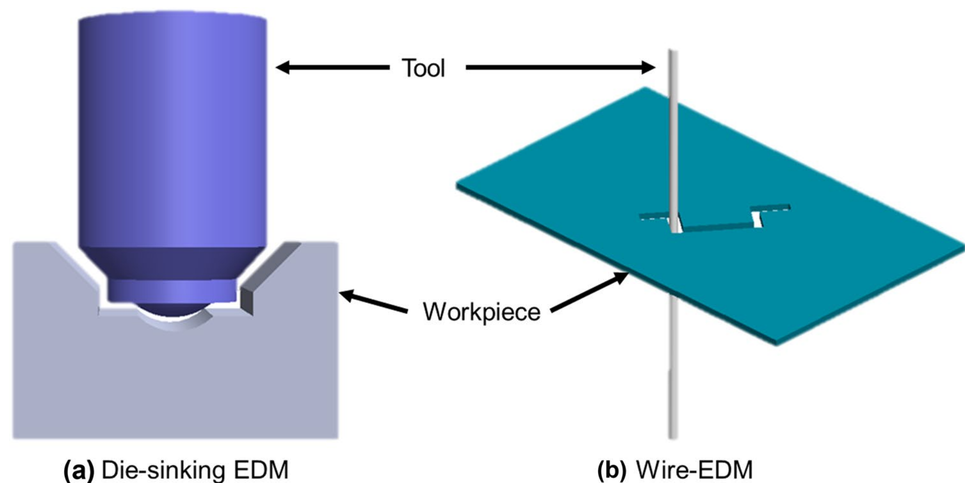

Fig. 9 Types of EDM (**a**) die-sinking and (**b**) wire-EDM. Source: own authors

monocrystalline Si ingots, the amount of sliced wafers can only be processed serially (one by one). In 2008, Okamoto et al. [120] reported a multi Wire-EDM to improve the wafer slicing process efficiency.

The machining performance of the surface quality is one of the important results that need to be investigated to obtain high aspect ratio structures. To study the process performance towards surface quality, the machining process of polished single-crystal Si plates using Wire-EDM were performed in water and oil [121, 122]. Figure 10b shows the Si machining results in water and oil, which revealed that the surface cutting in oil gave a smoother and better surface. Cutting in water was discovered to generate chips and cracks on the polished surface, which results in a very rough surface finish. Huijun et al. [123] studied the Si surface after being cut by Wire-EDM. The experimental results analyzed showed that the small holes (Fig. 10c) appeared on the surface caused by thermal stress damage and increased the crack propagation. Joshi et al. [124] studied the effect of Wire-EDM parameters on the surface quality, and wafer-thickness variation of the Si wafer using Wire-EDM. The surface roughness results were found in the range of 1–2.3 µm, and the wafer thickness variation can be reduced by increasing the wire tension, wire feed, and dielectric flushing pressure. Salleh et al. [125] demonstrated a 3D prototype of electrostatic micro-actuator fabrication using µ-Wire-EDM. The fabricated actuator has a long rod with a length of 2 mm, a width of 400 µm, and a pitch width between tooth of 650 µm.

The µEDM offers a micron range size, discharge energy, and axis movement, which is believed to produce micro-scale components and structures, with high accuracy results [126]. Masaki et al. [127] reported the first use of die-sinking μEDM for machining Si wafers. The authors asserted that the Si wafer could be machined using μEDM, but with a high incidence of short-circuits during the machining process. The die-sinking EDM machining technique is also seen to be capable in machining 3D and complex Si microstructure shapes [128–130]. Murray et al. [131] characterized the nano-scale damage such as pores, on machined Si surfaces using the EDM. Figure 10d shows a micrograph of a 100-µm depth hole machined on a n-type Si using the EDM, with positive tool polarity settings. The results showed that the pores with sizes of 10 and 200 nm, were formed on the machined surface.

The electrical conductivity of the workpiece material is the primary factor for machining using the EDM technique.

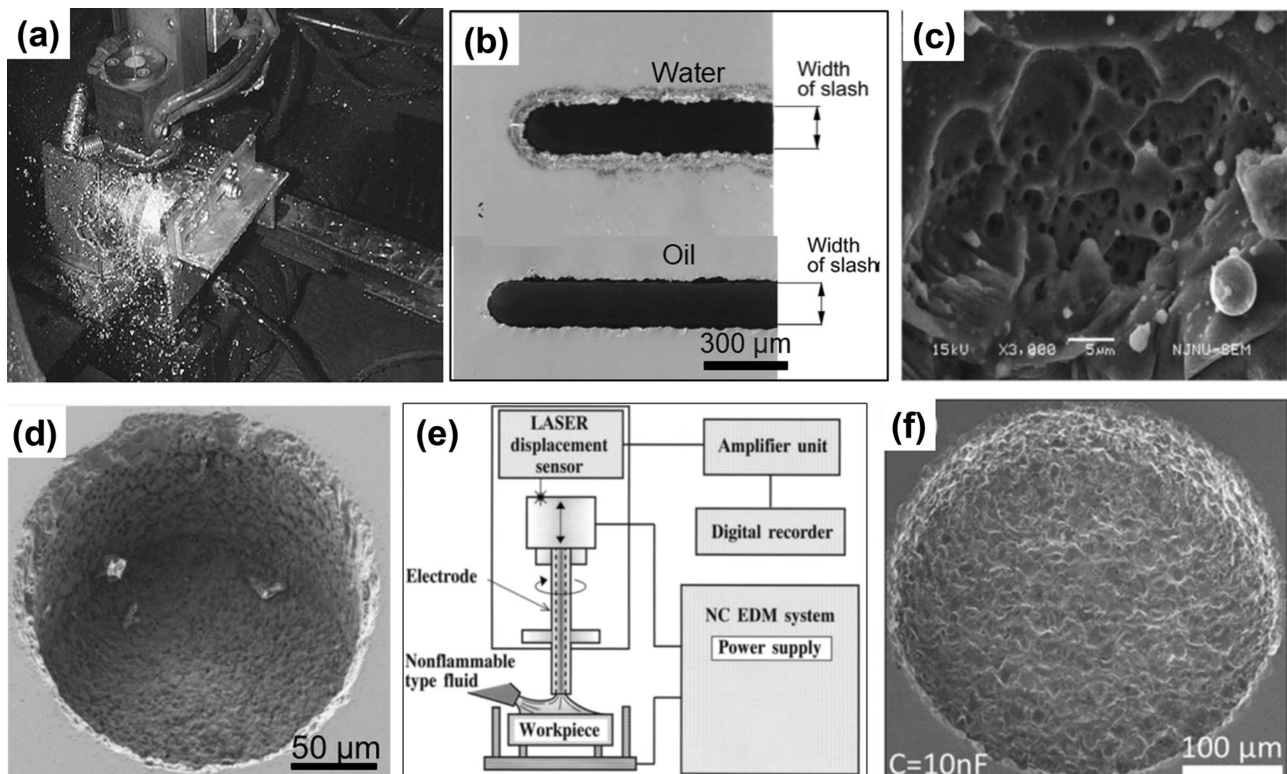

Fig. 10 Machined Si by EDM (**a**) Wire-EDM of water flushing. Source: adapted from Peng and Liao [119]; (**b**) Surface cut in water and oil by Wire-EDM. Source: adapted from Takino et al. [121]; (**c**) Small holes in bottom discharge pits. Source: adapted from Huijun et al. [123]; (**d**) Machined hole on n-type Si by die-sinking EDM. Source: adapted from Murray et al. [131]; (**e**) Schematic diagram setup of die-sinking EDM. Source: adapted from Uno et al. [132]; (**f**) Machined cavity by die-sinking µEDM process. Source: adapted from Daud et al. [135]

The surface potential barriers which prevent discharge currents in Si can be solved by plating or coating the material with a conductive layer. Luo et al. [117] introduced Ni plating to minimize surface contact resistance. As a result, the cutting rate increased after eliminating the surface potential barriers in Si machining. Improvement works on machining rates in the EDM machining have been investigated using Cu plates, by Uno et al. [132]. Figure 10e shows a schematic diagram of the EDM experimental setup for providing a transistor switching and condenser circuit. Kuneida and Ojima [133] reported on the impurities doped Al and Sb-Au into p-type and n-type Si wafers, respectively.

Temporary conductive Au coated on p-type Si wafer using μEDM and μ-Wire-EDM setup has also been reported [125, 134]. The machining stability was improved (~100× different machining conditions), and the performance of the MRR increased by a good margin (~30% average), compared to uncoated Si. Moreover, the authors also claimed that the machining process was stable without any short circuit. In 2018, the die-sinking μ-EDM performance for different resistivities of Si wafers was characterized by Daud et al. [135]. Figure 10f shows the machined cavity of low-resistivity Si with 50 μJ of DE. The study revealed that the electrical resistivity and the DE value had a great influence on the machining performance results. Recently in 2021, an investigation on heat assisted μ-EDM of lightly doped silicon was reported. The results showed that the machining rate was improved by a factor of ~16 times when machining at 250 °C, compared to room temperature [136]. The machining of Si wafers using EDM have been reported by previous researchers and is summarized in Table 4.

3 Comparison of non-traditional machining techniques

Non-traditional machining techniques such as USM, IBM, LBM, and EDM, provide an improved structure and surface quality, compared to traditional machining methods. Figure 11 summarizes the positive features and limitations of the non-traditional machining techniques. USM allows machining of all kinds of materials, be it hard, brittle, or fragile materials, including conductive materials. The USM technique is ideal for hard and brittle materials such as Si, borosilicate glass, Si nitride, quartz, and ceramics, to drill circular or non-circular holes, and produce precise machining [7, 11]. The MRR in this process is low, and the tool wear is high [7, 137]. In addition, deep hole machining is challenging due to abrasive slurry movements which are limited.

Similar to USM, the IBM technique also offers a low-temperature [138] process that minimizes the stress and thermal damage on the material [52]. However, it requires a high installation and equipment cost, very limited machining area, and extremely low MRR [139]. By contrast, the FIB milling, which transfers patterns with direct impingement of the ion beam on substrates, allows the creation of very shallow machining, less than 1 μm [45]. The surface material can be weakened by the radiation effects during the machining process. However, this machining method possesses extremely low MRR, that limits its application range.

LBM provides a range of positive features for the machining of hard and brittle materials like Si wafers, similar to USM. Moreover, the LBM is applicable for a wide range of materials [66]. There are no cutting forces involved in both LBM and IBM, because the energy is transferred by irradiation between the laser and the material [75, 93]. As a result, no material damage, tool wear, or machine vibration are caused by mechanical induces [66]. In addition, LBM is a flexible process that can be easily automated to manufacture fine structures with a high aspect ratio, and a machining starting point that can be easily located using a laser point. Nevertheless, despite being advantageous, the cost of the equipment required for the optical laser system is considered to be high [140]. In addition to thermal damage, tapered shapes are usually found in high depth machining, while adherent materials are normally found at the exit holes [140]. These two effects need to be addressed to achieve good quality structures.

Unlike other methods, EDM has proven to be more flexible and capable of machining 3D micro-structures and complex shapes across different materials [141]. The 3D design microstructures of bulk Si can be created with high precision EDM in a non-clean-room environment, and without photolithography facilities. Even so, hybrid techniques combining EDM with other traditional MEMS manufacturing methods deliver the best results in 3D Si processing [142]. Another significant positive feature of EDM is its ability to machine any conductive material, regardless of its hardness, brittleness, and toughness, which is difficult for other machining methods [113, 131, 143]. In addition, the EDM technique uses non-contact electrothermal machining, which allows the machining of hard and brittle materials, similar to USM and LBM. The minimum cutting forces of EDM provides the ability to avoid crack formation on the surface of the material, and to achieve good machining quality [144]. Moreover, EDM has relatively low equipment costs, and is environmentally friendly due to chemical-free processes. Furthermore, the fabrication process of tool electrodes is easier compared to other machining methods. However, EDM only operates efficiently on the conductive materials and its thermal action results in relatively low machining speeds [145]. Apart from that, additional time is needed, as the electrode wear of the EDM machine decreases during the machining process, and the power consumption of the EDM is considerably higher.

Table 4 Summary of machined Si wafer using the EDM

References	Type of EDM	Si wafer properties	Tool/wire properties	Machining settings	MRR	SR	Comments
[127]	μEDM	p-type 10-100Ω.cm <111> 330 μm thickness	W D-35–50 μm	100 V, 200 pF 2 μm /sec	N/A	N/A	Machine 340 μm depth of hole
[117]	Wire-EDM	n-type single-crystal ingot 7-15Ω.cm	Mo D-0.05–0.14 mm Tool negative: with, w/o Ni-plated, Tool positive: With, w/o Ni-plated	Traveling rate: 15 ms-1 Kerosene	MRR: 0.03 mm3/min	SR: 1.62 μm	Investigation of feasibility machine n-type Si with Ni-plated Cutting Rate: 170 mm2 min-1
[113]	EDM	n-type 4Ω.cm 380 μm thickness	W D-150 μm	40 rpm Min 0.8A Max 30A	MRR: 3.82 × 10–3 mm3/min	SR: 0.47–0.51 μm	Machine hole: -Diameter 160 μm -Depth 380 μm
[128]	μEDM	n-type 50mΩ.cm 350 μm thickness	W wire D-50 μm	40 rpm Min 0.8A Max 30A	N/A	SR: 0.011 μm	Machine Conical hole (angle 60°) 521 μm top 129 μm bottom
[132]	EDM	p-type mono-crystalline ingot 0.01Ω.cm 5 mm thickness	Cu D-1 mm 90 rpm Tool positive	380 pF 2, 6, 15 A non-flammable type liquid	MRR: 47.31 mm3/min	SR: 18 μm	-Machine 200 mm depth of hole Cu plate -Removal rate: 1 mm/s
[118]	Wire-EDM	p-type mono-crystalline ingot	Mo Diameter: 180 μm Tool negative	100 V 10.0 ms-1 deionized water	MRR: 0.026 mm3/min	SR: 7.6 μm	-Slice Si ingot by Wire-EDM -Removal rate: 104 mm2 min-1,
[133]	EDM	p-type: 354Ω. cm n-type: 8.3Ω. cm 0.75 μm thickness	Cu D-1 mm Tool positive	Positive and negative polarity 280 V 3.5A EDM oil	MRR: 0.589 mm3/min	N/A	Improve machining performance of MRR
[149]	EDM	p-type polished 20 mΩ.cm 650 μm thickness	W D-0.15 mm	60,80,100, 160 V 1000 pF deionized water	N/A	N/A	To investigate on formation of micro-crack
[119]	Wire-EDM	p-type mono-crystalline ingot D-76.2 mm 30Ω.cm 250 μm	Cu wire 0.25 mm	deionized water kerosene	MRR: 107.6 mm3 min-1	SR: 3.8 um	Study on slice Si ingot by WEDM

Table 4 (continued)

References	Type of EDM	Si wafer properties	Tool/wire properties	Machining settings	MRR	SR	Comments
[121]	Wire-EDM	Polished Si plate 0.02 Ω.cm D-150 mm Thickness: 10 mm Polished 0.2 nm	Brass D-200 µm	Water; 5A, 100 V, 1 µs, 83 kHz, 2 mm/min Oil; 30A, 150 V, 2 µs, 67 kHz, 1.8 mm/min	N/A	SR -Water: Rz 14.9 µm -Oil: Rz 16.4 µm	-Investigated the change in surface characteristic of Si in water and oil -Removal volume: -water 1.04 × 10 – 6 mm3/pulse -oil 1.17 × 10 – 6 mm3/pulse
[122]	Wire-EDM	Polished Si plate 0.02 Ω.cm D-100 mm Thickness: 10 mm Polished 0.2 nm	Brass D-200 µm	Water; 5 A, 100 V, 1 µs, 83 kHz Oil; 30A, 150 V, 2 µs, 67 kHz,	N/A	N/A	-Investigated on the surface treatment of Si surface cutting by WEDM-applied mask
[104]	EDM	n-type, Sb dopant 0.005–0.002 Ω.cm < 110 > 500–550 µm thickness D-4 inch (original) 12 mm round pieces	-WC electrode: D-0.03,0.05 mm -Graphite-Cu D-0.45 mm -Tool positive and negative	45 V 0.3A Pulse on: 15µsec Pulse off: 600µsec	MRR: - D-30 µm: 1.55 × 10–3 mm3 min-1 -D-50 µm: 3.6 × 10–3 mm3 min-1	N/A	-Machining micro hole and array micro holes
[120]	Wire-EDM	mono-crystalline ingot 0.01 Ω.cm, 2–3 Ω.cm 80 mm thickness	Mo D-180 µm Tension: 15 N Speed: 100–600 m. min-1 Tool negative	tool negative 100–120 V 3–8 A 400, 500, 600 m min-1 Deionized water	MRR: 0.18 mm3 min-1	SR: Rz 8 µm	-Proposed new slicing Si ingot method
[150]	-Wire-EDM -HS-Wire-EDM -Wire electrolytic-spark hybrid	n-type 0.5-3Ω.cm < 111 > 100 mm thickness	Wire-EDM: Cu–Zn-0.2 mm; HS-WEDM: Mo-0.18 mm; Wire EHM: Mo-0.18 mm Tool negative	Speed: Wire-EDM: < 0.2 ms-1, deionized water; HS-WEDM: 8-12 ms-1, water, oil, emulsifier, Wire EHM: adjustable, hybrid electrolyte	N/A	SR: 4.32 µm	-Investigated on slicing Si ingot by Wire electrolytic-spark hybrid, multi-wire saw, high speed wire-EDM
[123]	Wire-EDM	p-type 2.1Ω.cm 20 × 10x10 mm	Mo wire D-0.18 mm	-80 V,20 µs pulse width -130 V,20 µs pulse width -170 V,5 µs pulse width -Special dielectric fluid	N/A	N/A	-Analysis of damage mechanism on Si surface cutting by Wire-EDM

Table 4 (continued)

References	Type of EDM	Si wafer properties	Tool/wire properties	Machining settings	MRR	SR	Comments
[144]	EDM	p-type mono-crystalline 2.1 Ω.cm 8 mm thickness Conduction material: Fe	brass D-1.0 mm Tool positive and negative	150 V Pulse duration: 30 µs Penetrating speed: 533 µm min-1 Pure water	MRR: 0.0628 mm3 min-1 (positive polarity)	N/A	-Investigate on unidirectional conductivity of Si by EDM -1.2 mm through holes Metal (Fe) clamp
[131]	µEDM	n-type mono-crystalline ≤ 0.02 Ω.cm < 100 > 500 µm thickness	W D-150 µm Tool positive	90 V 1000pF Kerosene oil	MRR: 1.4544 × 10–3 mm3 min-1	N/A	-Characterize microstructural damage in Si
[134]	µ-Wire-EDM	p-type polished 1-50Ω.cm 650 µm thickness Au coated	Zn coated brass D-70 µm	85, 95, 105 V 0.1, 1, 10 nF 50micron sec-1	MRR: 0.002 mm3 min-1	N/A	-Investigate on machining performances of Si using temporary Au coated -1 mm L of slot
[151]	Wire-EDM	n-type mono-crystalline 0.001–0.005 Ω.cm < 100 > 508 µm thickness	brass wire D-250 µm tension 1 kg	70, 95, 120, 145 V 70 mm s-1 Deionized water	MRR: 4.8 mm3 min-1	SR: 5 µm, 20 µm	-Study on influence of machining parameters on cut surface characteristics and damage of Si
[152]	Wire-EDM	n-type mono-crystalline 0.001–0.005 Ω.cm < 100 > 508 µm thickness	brass wire D-250 µm tension 1 kg	70, 95, 120, 145 V 70 mm s-1 Deionized water	MRR: 4.8 mm3 min-1	SR: 5 µm, 20 µm	-Investigated on cut surface characteristic of Si and damage
[125]	µEDM µ-Wire-EDM	p-type polished 1-50Ω.cm 650 um thickness	W, 500um Zn coated brass, 70um	85, 95, 105 V 0.1, 1, 10nF 5um sec-1	MRR: -2 × 10–3 mm3 min-1 (µ-WEDM) -1.5 × 10–3 mm3 min-1 (µ-EDM)	N/A	-Improve performances-temporary Au coated -50 um depth hole (µEDM) -1 mm length cut (µWEDM)
[135]	µEDM	n-type mono-crystalline 0.001–0.005, 1–10 Ω.cm < 100 > 500 µm thickness	brass D-300 µm Tool negative	80,90,100,110,120 V 0.1,1,10,100,400 nF 50 µm min-1 3000 rpm dielectric oil, DIEL MS 5000	MRR: -3.505 × 10–3 mm3 min-1 (0.001–0.005 Ω.cm) -3.0294 × 10–3 mm3 min-1 (1–10 Ω.cm)	SR: -0.6466 µm (0.001–0.005 Ω.cm) -0.6203 µm (1–10 Ω.cm)	-Study on different resistivities and DE of Si machining by µEDM -100 µm depth of cavity
[124]	Wire-EDM	p-type poly Si 150 µm thickness	Brass wire D-100 µm Tool negative	45, 47 V Feed: 77, 137, 197 mm. min-1 Wire tension 0.3–0.5 kg Deionized water	MRR: 7.7754 × 10–5 mm3 min-1	SR: 1–2.3 µm	-Study on surface quality and different thickness of Si by Wire-EDM

Table 4 (continued)

References	Type of EDM	Si wafer properties	Tool/wire properties	Machining settings	MRR	SR	Comments
[136]	µEDM	p-type 500 µm thickness 1–10 Ω.cm	Brass tool D-150 µm Tool positive	100 V, 10 nF	MRR: 1.43 × 10–5	SR: 1.487 µm	-Study on proposed heat-assisted µEDM and analysis data of machining performances

Table 5 describes each of the machining methods discussed above. Four different non-traditional Si processing methods have been addressed in the previous section, namely USM, IBM, LBM and EDM. This machining types can be categorized based on the energy source, with micro-USM being identified as a mechanical machining type, while thermal machining involves LBM and EDM. The material removal concepts for EDM applies the thermal reaction of melting to the material erosion, while the laser beam applies the concept of a coherent and electromagnetic radiation beam to focus on the output material. USM uses tool oscillation at ultrasonic frequencies, while ion beam milling requires ion collisions to remove the material during the machining processes. The heat source required for the EDM process is from plasma, while photons act as a heat source in LBM. For IBM, it is not thermal, and is derived from ions. Since USM and IBM are not thermal machining, no heat source is needed, but USM required abrasives of solid grains, and IBM needs ions for the material removal process.

The machining medium is different for each machining type, which involves dielectric fluids for EDM, where the

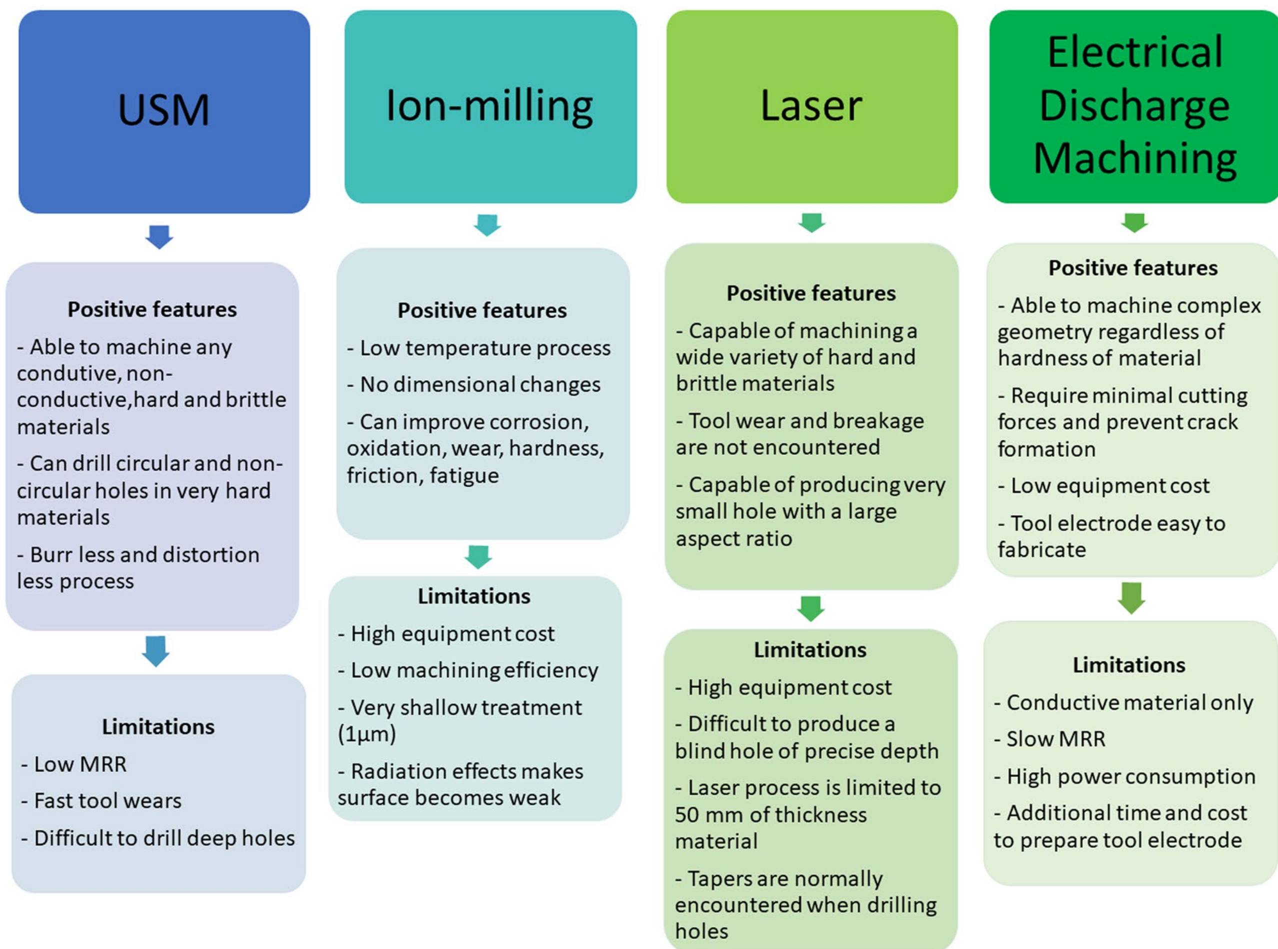

Fig. 11 Benefits and limitations of the four non-traditional machining techniques. Source: own authors

Table 5 Summary of non-traditional machining on Si

Features	USM	IBM	LBM	EDM
Source of energy	Mechanical	Ions	Thermal	Thermal
Energy sources	Abrasions	Ion beam	Laser beam	Electrical Discharges
Material removal source	Abrasives	Ions	Photons	Plasma
Machining medium of workpiece	Slurry	Vacuum	Air	Dielectric fluid
Principal of removal	Oscillation	Collision	Ablation	Melting
Contact with material	Yes	No	No	No
Tool wear	Yes	No	No	Yes
Equipment cost	High	High	High	Moderate
Material	Conductive, nonconductive, hard and brittle	Metals, semiconductor	Metals, polymers, ceramics	Only conductive materials
Thermal damage on workpiece	No	Yes (less)	Yes	Yes (less)
Machining range	Large	Small	Large	Large
Machining Resolution	20–100 µm	0.01–0.1 µm	> 5 µm	6.7–1000 µm

tool and workpiece are submerged inside, while the LBM is performed in an air medium. IBM is carried out in vacuum and slurry, which is the machining medium in USM. Since EDM, LBM and IBM involve thermal processes, thermal damage may occur to the surface material. In IBM, less damage is caused by the energy used, compared to EDM and LBM. The high equipment cost for USM, IBM and LBM is one of the main disadvantages of these techniques. The equipment cost for EDM is comparatively lower than others. However, EDM is mostly limited to conductive materials, compared to USM, LBM and IBM, of which, any materials can be machined regardless of their conductivity. Additionally, the machining range of the EDM, LBM and USM is considerably greater than that of the IBM. The machining dimensions reported by IBM seem to be the smallest;0.01–0.1 µm [3], LBM is > 5 µm [3], EDM is 6.7–1000 µm [3, 146] and USM is 20–100 µm [126].

4 Current status and future trends for non-traditional machining of Si

An analysis on research outputs on these mentioned non-traditional machining processes was obtained from the SCOPUS database (data collection date: February 15, 2021). The information was obtained using specific keywords, such as "micromachining silicon ultrasonic," "micromachining silicon Ion beam," "micromachining silicon laser beam," and "micromachining silicon electrical discharge machine," to gather research articles related to USM, IBM, LBM, and EDM of Silicon. Figure 12a shows the yearly distribution of the published research articles related to the above mentioned four processes over the last three decades. It can be inferred from Fig. 12, that research articles published on non-traditional micromachining of Si is more skewed towards LBM related studies, as compared to the other three methods. Figure 12b shows the total citation counts of these articles to date, suggesting that LBM contributes to the most significant portion of the complete citation (60%). To understand how research related to each of the four processes is distributed globally, Fig. 13a–d was generated. The data suggests that in terms of global prominence, Si's LBM machining is much more attractive to researchers worldwide. Based on our literature review and analysis, it can be fairly said that LBM machining of Si is much more dominant among the four non-traditional machining techniques

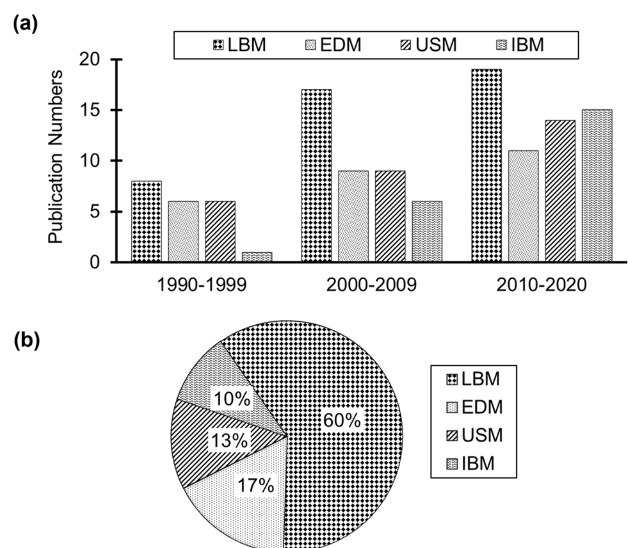

Fig. 12 (**a**) Distribution of number of SCOPUS indexed research articles published on four machining process over the last three decades (**b**) Citation count distribution for the research articles published in the field of LBM, EDM, USM and IBM machining of Silicon (1990-till to date). Source: own authors

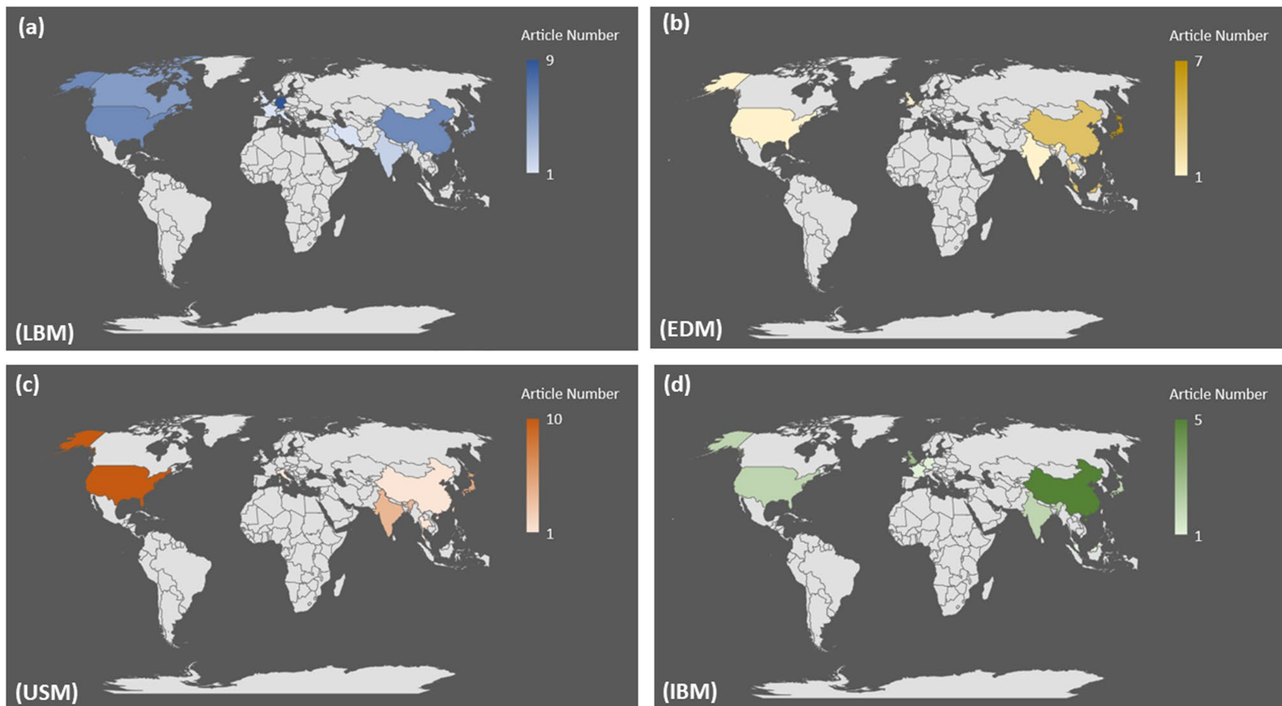

Fig. 13 How research related to LBM, EDM, USM and IBM machining of Si is distributed globally (**a**) LBM, (**b**) EDM, (**c**) USM and (**d**) IBM. Source: own authors

of Si, which we have discussed in this review article. The reason for researchers' interest in the LBM process is perhaps related to the significant advancement of the laser processing systems [147]. Laser machining is used not only for Silicon micromachining, but also in other fields, such as micro-optics, micro-biology, and micro-chemistry [148]. Based on the above discussion, it can be reasonably argued that the LBM process is the future trend for the micromachining of Si.

5 Conclusions

The Si material has been commonly used for electronic devices and MEMS applications due to its outstanding properties, which can be easily configured. Apart from that, the high demand for Si 3D microstructures with a high aspect ratio has driven both conventional and non-traditional machining techniques to its maximum potential. The description of the main features, performance, and implementation of the non-traditional machining techniques, namely USM, IBM, LBM and EDM, in Si machining were discussed in detail in this review paper. The entire discussion on the machining techniques of Si were focused on the working principles, types, performance, and examples of the reported machining Si structures. Thermal or heat utilization in the machining techniques for IBM, LBM, and EDM, the formation of the cracks, may affect the workpiece, especially for Si. In USM, the mechanical abrasion of solid grains can affect the workpiece surface. Despite the challenges in producing high quality Si microstructures, and the selection of a good machining techniques with optimum parameters, the LBM and EDM techniques are the preferred non-traditional machining methods. Non-contact machining features provided by LBM and EDM makes them much favorable Si machining techniques for industrial applications. Moreover, the thermal effects and cracks can be minimized in Si microstructures, when using these machining techniques. Although LBM is one of the chosen Si micromachining techniques among researchers, EDM offers more advantages in terms of equipment cost, minimizing the heat-affected zones, and is much more environmentally friendly. However, research is still on-going, and the main challenges to transfer the technology into the real world need to be addressed.

Acknowledgements This work was financially supported by Universiti Teknologi Malaysia under Industry-International Incentive Grant (Q.J130000.3651.02M36) and the Ministry of Education Malaysia under MyBrain scheme.

Author contribution [Noor Dzulaikha Daud], [Mohamed Sultan Mohamed Ali], [Md. Nazibul Hasan], [Tanveer Saleh] and [Pei Ling Leow] contributed to the study conception and manuscript writing. Material preparation, data collection and analysis were performed by [Noor Dzulaikha Daud], and [Md. Nazibul Hasan]. The major part of the manuscript was written by [Noor Dzulaikha Daud] and [Mohamed Sultan Mohamed Ali]. All authors contributed in preparing the manuscript. The final manuscript was read and approved by all authors.

Declarations

Ethics approval This paper does not contain any studies with human participants or animals.

Consent to participate This work does not involve human subjects.

Consent for publication This work does not involve human subjects.

Conflict of interest The authors declare no competing interests.

References

1. Sahu AK, Malhotra J, Jha S (2022) Laser-based hybrid micromachining processes: A review. Opt Laser Technol 146:107554
2. de Rooij N (1995) Current applications of silicon based microsystems. Micro Machine and Human Science, 1995 MHS'95, Proceedings of the Sixth International Symposium on: IEEE, p. 7–10
3. El-Hofy HA-G (2005) Advanced machining processes: nontraditional and hybrid machining processes. McGraw Hill Professional
4. Daud ND, Hasan MN, Ali MSM (2021) Microelectrical discharge machining of silicon wafers. Micro Electro-Fabrication. Elsevier, p. 219–44
5. Gentili E, Tabaglio L, Aggogeri F (2005) Review on micromachining techniques. Springer
6. Hasan MN, Ali MSM (2021) Electrical discharge machining for the formation of bulk-shape memory alloy actuators. Micro Electro-Fabrication. Elsevier, p. 195–217
7. Thoe TB, Aspinwall DK, Wise MLH (1998) Review on ultrasonic machining. Int J Mach Tools Manuf 38(4):239–255. https://doi.org/10.1016/S0890-6955(97)00036-9
8. Mirad MM, Das B (2021) A critical review of the state of the art literature in the monitoring of ultrasonic machining process and tool failure prediction. Eng Fail Anal 130:105769
9. Jain V, Sharma AK, Kumar P (2011) Recent developments and research issues in microultrasonic machining. ISRN Mech Eng
10. Kremer D, Saleh S, Ghabrial S, Moisan A (1981) The state of the art of ultrasonic machining. CIRP Ann Manuf Technol 30(1):107–110
11. Sun X-Q, Masuzawa T, Fujino M (1996) Micro ultrasonic machining and self-aligned multilayer machining/assembly technologies for 3D micromachines. Micro Electro Mechanical Systems, 1996, MEMS'96, Proceedings An Investigation of Micro Structures, Sensors, Actuators, Machines and Systems IEEE, The Ninth Annual International Workshop on: IEEE, p. 312–7
12. Sun X-Q, Masuzawa T, Fujino M (1996) Micro ultrasonic machining and its applications in MEMS. Sens Actuators A 57(2):159–64
13. Moreland M (1988) Versatile performance of ultrasonic machining. Am Ceram Soc Bull 67(6):1045–1047
14. Koval'chenko M, Paustovskii A, Perevyazko V (1986) Influence of properties of abrasive materials on the effectiveness of ultrasonic machining of ceramics. Soviet Powder Metall Metal Ceram 25(7):560–562
15. Moore D (1985) Ultrasonic impact grinding. Nontraditional Mach 137–9
16. Gilmore R (1990) Ultrasonic machining and orbital abrasion techniques. Soc Manuf Eng Trans Best Pap 1989 20
17. Neppiras E, Foskett R (1957) Ultrasonic machining-II. Operating conditions and performance of ultrasonic drills. Philips Tech Rev 18(12):368–79
18. Yu Z, Hu X, Rajurkar KP (2006) Influence of debris accumulation on material removal and surface roughness in micro ultrasonic machining of silicon. CIRP Ann Manuf Technol 55(1):201–204. https://doi.org/10.1016/S0007-8506(07)60398-9
19. Cong W, Feng Q, Pei Z, Deines TW, Treadwell C (2012) Edge chipping in rotary ultrasonic machining of silicon. Int J Manuf Res 7(3):311–329
20. Guzzo PL, Raslan A, De Mello JDB (1999) Relationship between quartz crystal orientation and the surface quality obtained by ultrasonic machining. Frequency and Time Forum, 1999 and the IEEE International Frequency Control Symposium, 1999, Proceedings of the 1999 Joint Meeting of the European: IEEE, p. 792–5
21. Yan BH, Wang AC, Huang CY, Huang FY (2002) Study of precision micro-holes in borosilicate glass using micro EDM combined with micro ultrasonic vibration machining. Int J Mach Tools Manuf 42(10):1105–1112. https://doi.org/10.1016/S0890-6955(02)00061-5
22. Kumar J, Khamba J, Mohapatra S (2008) An investigation into the machining characteristics of titanium using ultrasonic machining. Int J Mach Mach Mater 3(1–2):143–161
23. Ghahramani B, Wang ZY (2001) Precision ultrasonic machining process: a case study of stress analysis of ceramic (Al2O3). Int J Mach Tools Manuf 41(8):1189–1208. https://doi.org/10.1016/S0890-6955(01)00011-6
24. Khoo C, Hamzah E, Sudin I (2008) A review on the rotary ultrasonic machining of advanced ceramics. Jurnal Mekanikal 25:9–23
25. Farago FT (1976) Abrasive methods engineering. Industrial Press
26. Balamuth L (1964) Ultrasonic vibrations assist cutting tools. Metalwork Prod 108(24):75–77
27. Wang J, Zhang J, Feng P, Guo P (2018) Damage formation and suppression in rotary ultrasonic machining of hard and brittle materials: a critical review. Ceram Int 44(2):1227–1239
28. Egashira K, Masuzawa T (1999) Microultrasonic machining by the application of workpiece vibration. CIRP Ann Manuf Technol 48(1):131–134. https://doi.org/10.1016/S0007-8506(07)63148-5
29. Komaraiah M, Narasimha Reddy P (1993) A study on the influence of workpiece properties in ultrasonic machining. Int J Mach Tools Manuf 33(3):495–505. https://doi.org/10.1016/0890-6955(93)90055-Y
30. Endo T, Tsujimoto T, Mitsui K (2008) Study of vibration-assisted micro-EDM—The effect of vibration on machining time and stability of discharge. Precis Eng 32(4):269–277. https://doi.org/10.1016/j.precisioneng.2007.09.003
31. Egashira K, Masuzawa T, Fujino M, Sun X-Q (1997) Application of USM to micromachining by on-the-machine tool fabrication. Int J Electr Mach 2:31–36
32. Yu Z, Rajurkar K, Tandon A (2004) Study of 3D micro-ultrasonic machining. J Manuf Sci Eng 126(4):727–732
33. Tsui C-Y, Wu C-C, Lu M-C, Huang C-F (2008) Drilling of microholes on silicon wafer with ultrasonic workpiece holder. ASME 2008 International Design Engineering Technical Conferences and Computers and Information in Engineering Conference: American Society of Mechanical Engineers, p. 811–7
34. Zarepour H, Yeo S (2012) Single abrasive particle impingements as a benchmark to determine material removal modes in micro ultrasonic machining. Wear 288:1–8
35. Sreehari D, Sharma AK (2018) On form accuracy and surface roughness in micro-ultrasonic machining of silicon microchannels. Precis Eng 53:300–309
36. Kumar S, Dvivedi A (2019) On machining of hard and brittle materials using rotary tool micro-ultrasonic drilling process. Mater Manuf Processes 34(7):736–748
37. Castaing R, Laborie P (1953) Examen direct des métaux par transmission au microscope électronique. Comptes

Rendus Hebdomadaires des Seances de L academie des Sciences 237(21):1330–1332
38. Paulus M, Reverchon F (1961) Dispositif de bombardement ionique pour préparations micrographiques. J Phys Appl 22(S6):103–107
39. Heaney PJ, Vicenzi EP, Giannuzzi LA, Livi KJ (2001) Focused ion beam milling: A method of site-specific sample extraction for microanalysis of Earth and planetary materials. Am Miner 86(8–9):1094–1099
40. Barber D (1999) Development of ion-beam milling as a major tool for EM. Microsc Anal 5–10
41. McGeough JA (1988) Advanced methods of machining. Springer Science & Business Media
42. Amirmajdi OM, Ashyer-Soltani R, Clode MP, Mannan SH, Wang Y, Cabruja E et al (2009) Cross-section preparation for solder joints and MEMS device using argon ion beam milling. IEEE Trans Electron Packag Manuf 32(4):265–271
43. Preiß EI, Merle B, Xiao Y, Gannott F, Liebig JP, Wheeler JM et al (2021) Applicability of focused Ion beam (FIB) milling with gallium, neon, and xenon to the fracture toughness characterization of gold thin films. J Mater Res 36(12):2505–2514
44. Pastewka L, Salzer R, Graff A, Altmann F, Moseler M (2009) Surface amorphization, sputter rate, and intrinsic stresses of silicon during low energy Ga+ focused-ion beam milling. Nucl Instrum Methods Phys Res Sect B 267(18):3072–3075
45. Tseng AA (2004) Recent developments in micromilling using focused ion beam technology. J Micromech Microeng 14(4):R15
46. Hung N, Fu Y, Ali MY (2002) Focused ion beam machining of silicon. J Mater Process Technol 127(2):256–260
47. Giannuzzi L, Prenitzer B, Drown-MacDonald J, Shofner T, Brown S, Irwin R et al (1998) Electron microscopy sample preparation for the biological and physical sciences using focused ion beams. AT PROCESS 4:162–167
48. Chen Y, Zhang X (2010) Focused ion beam technology and application in failure analysis. Electronic Packaging Technology & High Density Packaging (ICEPT-HDP), 2010 11th International Conference on: IEEE, p. 957–60
49. Tseng AA (2005) Recent developments in nanofabrication using focused ion beams. Small 1(10):924–939
50. Takahashi H, Sato A, Takakura M, Mori N, Boerder J, Knoll W et al (2006) A new method of surface preparation for high spatial resolution EPMA/SEM with an argon ion beam. Microchim Acta 155(1–2):295–300
51. Bhavsar SN, Aravindan S, Rao PV (2014) Machinability study of high speed steel for focused ion beam (FIB) milling process–An experimental investigation at micron/nano scale. Precis Eng 38(1):168–173
52. Tang L, Zhang Y, Bosman M, Woo J (2010) Study of ion beam damage on FIB prepared TEM samples. Physical and Failure Analysis of Integrated Circuits (IPFA), 2010 17th IEEE International Symposium on the: IEEE, p. 1–4
53. Ali MY, Loo YW (2007) Geometrical integrity of micromold cavity sputtered by FIB using multilayer slicing approach. Microsyst Technol 13(1):103–107
54. Youn S-W, Okuyama C, Takahashi M, Maeda R (2008) A study on fabrication of silicon mold for polymer hot-embossing using focused ion beam milling. J Mater Process Technol 201(1):548–553
55. Chew NG, Cullis AG (1987) The preparation of transmission electron microscope specimens from compound semiconductors by ion milling. Ultramicroscopy 23(2):175–198. https://doi.org/10.1016/0304-3991(87)90163-X
56. Giannuzzi LA, Drown JL, Brown SR, Irwin RB, Stevie FA (1998) Applications of the FIB lift-out technique for TEM specimen preparation. Microsc Res Tech 41(4):285–290
57. Hopman WC, Ay F, Hu W, Gadgil VJ, Kuipers L, Pollnau M et al (2007) Focused ion beam scan routine, dwell time and dose optimizations for submicrometre period planar photonic crystal components and stamps in silicon. Nanotechnology 18(19):195305
58. Sabouri A, Anthony C, Bowen J, Vishnyakov V, Prewett P (2014) The effects of dwell time on focused ion beam machining of silicon. Microelectron Eng 121:24–26
59. Salvati E, Brandt L, Papadaki C, Zhang H, Mousavi S, Wermeille D et al (2018) Nanoscale structural damage due to focused ion beam milling of silicon with Ga ions. Mater Lett 213:346–349
60. Goswami A, Singh K, Aravindan S, Rao PV (2017) Optimizing FIB milling process parameters for silicon and its use in nanoreplication. Mater Manuf Processes 32(10):1052–1058. https://doi.org/10.1080/10426914.2016.1257127
61. Garg V, Mote RG, Fu J (2020) Facile fabrication of functional 3D micro-nano architectures with focused ion beam implantation and selective chemical etching. Appl Surf Sci 146644
62. Simon P, Ihlemann J (1996) Machining of submicron structures on metals and semiconductors by ultrashort UV-laser pulses. Appl Phys A 63(5):505–508
63. Bakhtiyari AN, Wang Z, Wang L, Zheng H (2021) A review on applications of artificial intelligence in modeling and optimization of laser beam machining. Opt Laser Technol 135:106721
64. Majumdar JD, Manna I (2003) Laser processing of materials. Sadhana 28(3–4):495–562
65. Chryssolouris G (1991) Laser Machining Theory and Practice. Springer-Verlag
66. Dubey AK, Yadava V (2008) Laser beam machining—A review. Int J Mach Tools Manuf 48(6):609–628. https://doi.org/10.1016/j.ijmachtools.2007.10.017
67. Muthuramalingam T, Akash R, Krishnan S, Phan NH, Pi VN, Elsheikh AH (2021) Surface quality measures analysis and optimization on machining titanium alloy using CO2 based laser beam drilling process. J Manuf Processes 62:1–6
68. Gautam GD, Pandey AK (2018) Pulsed Nd: YAG laser beam drilling: A review. Opt Laser Technol 100:183–215
69. Meijer J (2004) Laser beam machining (LBM), state of the art and new opportunities. J Mater Process Technol 149(1):2–17
70. Tabata N, Yagi S, Hishii M (1996) Present and future of lasers for fine cutting of metal plate. J Mater Process Technol 62(4):309–314. https://doi.org/10.1016/S0924-0136(96)02426-0
71. Faisal N, Zindani D, Kumar K, Bhowmik S (2019) Laser micromachining of engineering materials—a review. Micro Nano Mach Eng Mater 121–36
72. Goswami D, Chakraborty S (2015) A study on the optimization performance of fireworks and cuckoo search algorithms in laser machining processes. J Inst Eng (India) Ser C 96(3):215–29
73. Hamad AH (2016) Effects of different laser pulse regimes (nanosecond, picosecond and femtosecond) on the ablation of materials for production of nanoparticles in liquid solution. High Energy Short Pulse Lasers 305–25
74. Liu H-H, Hu Y, Cui H-P (2015) Femtosecond laser in refractive and cataract surgeries. Int J Ophthalmol 8(2):419
75. Venkatakrishnan K, Sudani N, Tan B (2008) A high-repetition-rate femtosecond laser for thin silicon wafer dicing. J Micromech Microeng 18(7):075032
76. Kasaai MR, Kacham V, Theberge F, Chin SL (2003) The interaction of femtosecond and nanosecond laser pulses with the surface of glass. J Non-Cryst Solids 319(1):129–135
77. Amer M, El-Ashry M, Dosser L, Hix K, Maguire J, Irwin B (2005) Femtosecond versus nanosecond laser machining: comparison of induced stresses and structural changes in silicon wafers. Appl Surf Sci 242(1):162–167
78. Dahotre NB, Harimkar S (2008) Laser fabrication and machining of materials. Springer Science & Business Media
79. Sugioka K, Cheng Y (2014) Femtosecond laser three-dimensional micro-and nanofabrication. Appl Phys Rev 1(4):041303

80. Voisey K, Cheng C, Clyne T (2000) Quantification of melt ejection phenomena during laser drilling. MRS Online Proc Libr Arch 617
81. Tahmouch G, Meyrueis P, Grandjean P (1997) Cutting by a high power laser at a long distance without an assist gas for dismantling. Opt Laser Technol 29(6):307–315
82. Chen T-C, Darling RB (2005) Parametric studies on pulsed near ultraviolet frequency tripled Nd: YAG laser micromachining of sapphire and silicon. J Mater Process Technol 169(2):214–218
83. Ghany KA, Newishy M (2005) Cutting of 1.2 mm thick austenitic stainless steel sheet using pulsed and CW Nd: YAG laser. J Mater Process Technol 168(3):438–47
84. Chen S-L (1999) The effects of high-pressure assistant-gas flow on high-power CO2 laser cutting. J Mater Process Technol 88(1–3):57–66
85. Krüger J, Kautek W (1995) Femtosecond-pulse laser processing of metallic and semiconducting thin films. Photonics West'95: International Society for Optics and Photonics, p. 436–47
86. Chichkov BN, Momma C, Nolte S, Von Alvensleben F, Tünnermann A (1996) Femtosecond, picosecond and nanosecond laser ablation of solids. Appl Phys A 63(2):109–115
87. Müllenborn M, Dirac H, Petersen JW, Bouwstra S (1996) Fast three-dimensional laser micromachining of silicon for microsystems. Sens Actuators A 52(1):121–5
88. Geng N, Fu X, Li H, Ni X, Hu XT (2007) Effect of laser parameters in the micromachining of silicon by femtosecond pulse laser. Key Eng Mater 339:136–140
89. Dauer S, Ehlert A, Büttgenbach S (1999) Rapid prototyping of micromechanical devices using a Q-switched Nd: YAG laser with optional frequency doubling. Sens Actuators A 76(1):381–5
90. Amer MS, Dosser L, LeClair S, Maguire JF (2002) Induced stresses and structural changes in silicon wafers as a result of laser micro-machining. Appl Surf Sci 187(3–4):291–296. https://doi.org/10.1016/S0169-4332(01)01043-1
91. Pan CT, Hwang YM, Hsieh CW (2005) Dynamic characterization of silicon-based microstructure of high aspect ratio by dual-prism UV laser system. Sens Actuators A 122(1):45–54. https://doi.org/10.1016/j.sna.2005.04.015
92. Tang Y, Fuh J, Loh H, Wong Y, Lim Y (2008) Laser dicing of silicon wafer. Surf Rev Lett 15(1–2):153–159
93. Kagerer M, Irlinger F, Lueth TC (2011) Laser source independent basic parameters in micro-cutting. Advanced Intelligent Mechatronics (AIM), 2011 IEEE/ASME International Conference on: IEEE, p. 391–6
94. Chung C, Wu M, Wu J, Sung Y, Huang G (2006) Silicon micromachining by CO_2 laser. Nano/Micro Engineered and Molecular Systems, 2006 NEMS'06 1st IEEE International Conference on: IEEE, p. 1445–8
95. Weinhold S, Gruner A, Ebert R, Schille J, Exner H (2014) Study of fast laser induced cutting of silicon materials. SPIE LASE: International Society for Optics and Photonics, p. 89671J-J-7
96. Wang F, Zhao L, Tu YP, Liu Y, Chen J-x (2017) Image feature analysis of plasma spot produced from femtosecond laser ablation for silicon wafer. J Micro/Nanolithogr MEMS MOEMS 16(2):025003
97. Goodarzi R, Hajiesmaeilbaigi F (2018) Circular ripple formation on the silicon wafer surface after interaction with linearly polarized femtosecond laser pulses in air and water environments. Opt Quantum Electron 50(7):299
98. Chen T-H, Fardel R, Arnold CB (2018) Ultrafast z-scanning for high-efficiency laser micro-machining. Light Sci Appl 7(4):17181-
99. Singh NK, Singh Y, Sharma A, Singla A, Negi P (2021) An environmental-friendly electrical discharge machining using different sustainable techniques: a review. Adv Mater Process Technol 7(4):537–566
100. Ramulu M, Taya M (1989) EDM machinability of SiCw/Alcomposites. J Mater Sci 24(3):1103–1108
101. König W, Dauw DF, Levy G, Panten U (1988) EDM-future steps towards the machining of ceramics. CIRP Ann Manuf Technol 37(2):623–631. https://doi.org/10.1016/S0007-8506(07)60759-8
102. Grigoriev SN, Hamdy K, Volosova MA, Okunkova AA, Fedorov SV (2021) Electrical discharge machining of oxide and nitride ceramics: A review. Mater Des 209:109965
103. Reynaerts D, Meeusen W, Song X, Van Brussel H, Reyntjens S, De Bruyker D et al (2000) Integrating electro-discharge machining and photolithography: work in progress. J Micromech Microeng 10(2):189
104. Weng FT, Hsu CS, Lin WF (2006) Fabrication of micro components to Silicon wafer using EDM process. Mater Sci Forum Trans Tech Publ 217–217
105. Abu Qudeiri JE, Saleh A, Ziout A, Mourad A-HI, Abidi MH, Elkaseer A (2019) Advanced electric discharge machining of stainless steels: Assessment of the state of the art, gaps and future prospect. Materials 12(6):907
106. Czelusniak T, Higa C, Torres R, Laurindo C, Paiva JM Jr, Lohrengel A et al (2019) Materials used for sinking EDM electrodes: a review. J Braz Soc Mech Sci Eng. https://doi.org/10.1007/s40430-018-1520-y
107. Rajurkar K, Sundaram M, Malshe A (2013) Review of electrochemical and electrodischarge machining. Procedia CIRP 6:13–26
108. Drozda T, Wick C, Bakerjian R, Benedict JT, Veilleux RF (1983) Tool and manufacturing engineers handbook: continuous improvement. Soc Manuf Eng
109. Muttamara A, Fukuzawa Y, Mohri N, Tani T (2009) Effect of electrode material on electrical discharge machining of alumina. J Mater Process Technol 209(5):2545–2552
110. Song X, Reynaerts D, Meeusen W, Van Brussel H (1999) Micro-EDM for silicon microstructure fabrication. Design, Test, and Microfabrication of MEMS/MOEMS: International Society for Optics and Photonics p. 792–9
111. Davis JR, Lampman S, Zorc T (1989) Metals Handbook. Vol. 16: Machining. ASM International, Metals Park, Ohio 44073, USA, 944
112. Tsai Y-Y, Masuzawa T (2004) An index to evaluate the wear resistance of the electrode in micro-EDM. J Mater Process Technol 149(1):304–309
113. Reynaerts D, Van Brussel H (1997) Microstructuring of silicon by electro-discharge machining (EDM)—part I: theory. Sens Actuators A 60(1):212–218
114. Luo Y (1995) An energy-distribution strategy in fast-cutting wire EDM. J Mater Process Technol 55(3):380–390
115. Suziki Y, Kishi M (1989) Improvement of Surface Roughness in wire EDM. Proceedings of the Ninth International Symposium for Electro-Machining (ISEM-9), Nagoya, Japan
116. Kalpakjian S (1997) Manufacturing Process for Engineering Materials. Addison-Wesley, Reading, MA
117. Luo Y, Chen C, Tong Z (1992) Investigation of silicon wafering by wire EDM. J Mater Sci 27(21):5805–5810
118. Uno Y, Okada A, Okamoto Y, Hirano T (2000) Wire EDM slicing of monocrystalline silicon ingot. Proc 2000 ASPE Annu Meet 172–175
119. Peng W, Liao Y (2003) Study of electrical discharge machining technology for slicing silicon ingots. J Mater Process Technol 140(1):274–279
120. Okamoto Y, Uno Y, Okada A, Ohshita S, Hirano T, Takata S (2008) Development of multi-wire EDM slicing method for silicon ingot. Proc ASPE Ann Meet 12th ICPE2008 530
121. Takino H, Ichinohe T, Tanimoto K, Yamaguchi S, Nomura K, Kunieda M (2004) Cutting of polished single-crystal silicon by wire electrical discharge machining. Precis Eng 28(3):314–319

122. Takino H, Ichinohe T, Tanimoto K, Yamaguchi S, Nomura K, Kunieda M (2005) High-quality cutting of polished single-crystal silicon by wire electrical discharge machining. Precis Eng 29(4):423–430. https://doi.org/10.1016/j.precisioneng.2004.12.004
123. Huijun P, Zhidong L, Lian G, Mingbo Q, Zongjun T (2013) Study of small holes on monocrystalline silicon cut by WEDM. Mater Sci Semicond Process 16(2):385–389
124. Joshi K, Bhandarkar UV, Joshi SS (2019) Surface integrity and wafer-thickness variation analysis of ultra-thin silicon wafers sliced using wire-EDM. Adv Mater Process Technol 5(3):512–525
125. Saleh T, Rasheed AN, Muthalif AG (2015) Experimental study on improving μ-WEDM and μ-EDM of doped silicon by temporary metallic coating. Int J Adv Manuf Technol 78(9–12):1651–1663
126. Masuzawa T (2000) State of the Art of Micromachining. CIRP Ann Manuf Technol 49(2):473–488. https://doi.org/10.1016/S0007-8506(07)63451-9
127. Masaki T, Kawata K, Masuzawa T (1990) Micro electro-discharge machining and its applications. Micro Electro Mechanical Systems, 1990 Proceedings, An Investigation of Micro Structures, Sensors, Actuators, Machines and Robots IEEE 1990:21–26
128. Reynaerts D, Meeusen W, Van Brussel H (1998) Machining of three-dimensional microstructures in silicon by electro-discharge machining. Sens Actuators A 67(1):159–165
129. Heeren P, Reynaerts D, Van Brussel H (1997) Three-dimensional silicon micromechanical parts manufactured by electro-discharge machining. Advanced Robotics, 1997 ICAR'97 Proceedings, 8th International Conference on: IEEE 1997 p. 247–52
130. Reynaerts D, Van Brussel H, Beuret C, Larsson O, Bertholds A (1997) Microstructing of silicon by electro-discharge machining (EDM)—part II: applications. Sens Actuators A 61(1):379–386
131. Murray J, Fay M, Kunieda M, Clare A (2013) TEM study on the electrical discharge machined surface of single-crystal silicon. J Mater Process Technol 213(5):801–809
132. Uno Y, Okada A, Okamoto Y, Yamazaki K, Risbud SH, Yamada Y (1999) High efficiency fine boring of monocrystalline silicon ingot by electrical discharge machining. Precis Eng 23(2):126–133. https://doi.org/10.1016/S0141-6359(98)00029-4
133. Kunieda M, Ojima S (2000) Improvement of EDM efficiency of silicon single crystal through ohmic contact. Precis Eng 24(3):185–190
134. Rasheed AN, Muthalif A, Gani A, Saleh T (2014) Improving μ-wire electro-discharge machining operation of polished silicon wafer by conductive coating
135. Daud ND, AbuZaiter A, Leow PL, Ali MSM (2018) The effects of the silicon wafer resistivity on the performance of microelectrical discharge machining. Int J Adv Manuf Technol 95(1–4):257–266
136. Daud ND, Ghazali FAM, Abd Hamid FK, Nafea M, Saleh T, Leow PL, Ali MSM (2021) Heat-assisted μ-electrical discharge machining of silicon. Int J Adv Manuf Technol 1–12
137. Asami T, Miura H (2012) Study of hole machining of brittle material by ultrasonic complex vibration. Ultrasonics Symposium (IUS), 2012 IEEE International: IEEE 2012 p. 2667–70
138. Atiqah N, Jaafar I, Ali MY, Asfana B (2012) Application of focused ion beam micromachining: a review. Adv Mater Res Trans Tech Publ 507–510
139. Meijer J, Du K, Gillner A, Hoffmann D, Kovalenko V, Masuzawa T et al (2002) Laser machining by short and ultrashort pulses, state of the art and new opportunities in the age of the photons. CIRP Ann Manuf Technol 51(2):531–550
140. Samant AN, Dahotre NB (2009) Laser machining of structural ceramics—A review. J Eur Ceram Soc 29(6):969–993. https://doi.org/10.1016/j.jeurceramsoc.2008.11.010
141. Ho KH, Newman ST (2003) State of the art electrical discharge machining (EDM). Int J Mach Tool Manuf 43(13):1287–1300. https://doi.org/10.1016/S0890-6955(03)00162-7
142. Chan M, Fonda P, Reyes C, Xie J, Najar H, Lin L et al (2012) Micromachining 3D hemispherical features in silicon via micro-EDM. Micro Electro Mechanical Systems (MEMS), 2012 IEEE 25th International Conference on: IEEE 2012. p. 289–292
143. Fonda P, Chan M, Heidari A, Nakamoto K, Sano S, Horsley D et al (2013) The application of diamond-based electrodes for efficient EDMing of silicon wafers for freeform MEMS device fabrication. Procedia CIRP 6:280–285
144. Mingbo Q, Zhidong L, Zongjun T, Wei W, Yinhui H (2013) Study of unidirectional conductivity on the electrical discharge machining of semiconductor crystals. Precis Eng 37(4):902–907
145. Patel D, Vaghmare V (2013) A Review of recent work in wire electrical discharge machining (WEDM). IJERA 3(3):805–816
146. Egashira K, Mizutani K (2002) Micro-drilling of monocrystalline silicon using a cutting tool. Precis Eng 26(3):263–268
147. Shannon G (2017) Ultrafast lasers offer great promise as a unique manufacturing tool. https://www.industrial-lasers.com/home/article/16490420/ultrafast-lasers-offer-great-promise-as-a-unique-manufacturing-tool. Accessed 24 Feb 2021
148. Mishra S, Yadava V (2015) Laser Beam MicroMachining (LBMM) – A review. Opt Lasers Eng 73:89–122. https://doi.org/10.1016/j.optlaseng.2015.03.017
149. Song X, Reynaerts D, Meeusen W, Van Brussel H (2001) A study on the elimination of micro-cracks in a sparked silicon surface. Sens Actuators A 92(1):286–291
150. Wang W, Liu ZD, Tian ZJ, Huang YH, Liu ZX (2009) High efficiency slicing of low resistance silicon ingot by wire electrolytic-spark hybrid machining. J Mater Process Technol 209(7):3149–3155. https://doi.org/10.1016/j.jmatprotec.2008.07.029
151. Punturat J, Tangwarodomnukun V, Dumkum C (2014) Surface characteristics and damage of monocrystalline silicon induced by wire-EDM. Appl Surf Sci 320:83–92
152. Punturat J, Tangwarodomnukun V, Dumkum C (2014) Investigation of process performances and cut surface characteristics in the wire-EDMing of silicon. Adv Mater Res 845:950–954

Publisher's Note Springer Nature remains neutral with regard to jurisdictional claims in published maps and institutional affiliations.